A dissertation entitled

GABOR LENS FOCUSING AND EMITTANCE

GROWTH IN A LOW ENERGY PROTON BEAM

submitted to the Graduate School of the
University of Wisconsin-Madison
in partial fulfillment of the requirements for the
degree of Doctor of Philosophy

by

John A. Palkovic

Degree to be awarded: December 19 91 May 19___ August 19___

Approved by Dissertation Readers:

Major Professor

July 22, 1991

Date of Examination

Dean, Graduate School

Abstract

We have measured emittances in a low energy proton beam at energies between 19 and 49 KeV and currents between 9 and 39 mA. We find that the rms emittance of the proton beam grew by an average amount of 60 % in a propagation distance of 2.5 cm. An Abel inversion procedure is applied to the charge distribution of the proton beam in order to calculate the electrostatic field energy of the beam. We find that all the emittance growth is due to $\simeq$ 10% of the beam particles. In addition, a study of low energy beam focusing in a Gabor lens was done. We show that the Gabor lens is not useful for focusing negative ion beams.

Acknowledgements

First and foremost, I would like to thank my wife Candace for all the love and support she gave me while I was writing this thesis. I would like to thank my advisors, Fred Mills and Keith Symon, for the guidance they gave and the consummate knowledge of accelerator physics which they showed. Don Young was a source of much inspiration to me, and a storehouse of knowledge on linear accelerators. I acknowledge useful discussions with Chuck Schmidt, James Rosenzweig, Frank Cole, Bob Noble, and Ping Zhou. I thank Michael Allen and Elliott McCrory for writing most of the computer programs used for the data acquisition. Many thanks to Jim Wendt and Ray Hren for all their help in the laboratory. I could not have done it without you. A heartfelt thanks goes out to the Universities Research Association and Fermilab for the use of the Fermilab facilities and their continuing support of the Fermilab fellowships in accelerator physics.

Dedication

To my wife Candace, my son Martin, my mother Gloria, my father John, my brothers Michael, Joseph, and James, and my sisters Karen, Mary, Therese, Anne, Jean, and Angela.

Contents

Abstract ii

Acknowledgements iii

Dedication iv

1 INTRODUCTION 1

1.1 Introduction 1

1.1.1 Motivation and Background 1

1.1.2 Summary of the Thesis 6

1.2 The Problem of Low-Energy Beam Transport 10

1.2.1 The Need For Intense Beams 10

1.2.2 Beam Optics and the Definition of Matching. 12

1.2.3 Emittance Growth of Space-Charge Dominated Beams. . . 15

1.2.4 Experimental Techniques Used with Space-Charge Dominated Beams 20

1.3 Lenses used in low-energy beam transport 22

1.3.1 Azimuthally symmetric lenses 22

1.3.2 Nonsymmetric Lenses 25

2 PHYSICS OF BEAMS WITH SPACE CHARGE 28

2.1 Characteristics of Space Charge Dominated Beams 28

2.1.1 Distribution Functions and Phase Space 28

2.1.2 Standard Beam Parameters 31

2.1.3 Liouville's Theorem and the Emittance 33

3 PHYSICS OF GABOR LENSES 37

3.1 Nonneutral Plasma Physics 37

3.1.1 The Brillouin Limit 38

3.1.2 Finite Temperature Equilibrium of a Nonneutral Plasma Column 42

3.1.3 On the Difficulty of Focusing Negative Ion Beams with a Gabor Lens 46

3.2 Focusing properties 47

3.2.1 The fields of the Nonneutral Column 47

4 EXPERIMENTAL RESULTS 49

4.1 Experimental Setup 49

4.1.1 Data Acquisition Electronics and Software 49

4.1.2 Ion Source Test Stand and Duoplasmatron 52

4.2 Gabor Lens 58

4.2.1 Design of the Gabor Lens 59

4.2.2 Magnetic Field of the Lens 60

4.3 Beam Measurements 62

4.3.1 Measurement of the Emittance 62
4.3.2 Abel Inversion of the Density Profile 64
4.3.3 Calculation of the Electrostatic Field Energy 70
4.3.4 Data Interpretation 71

5 CONCLUSION **87**

Bibliography **89**

List of Figures

1.1 Fermilab Gabor lens. 7

1.2 Evolution of the beam emittance in a uniform focusing channel. . 17

1.3 Electrostatic cylinder lens. 23

1.4 "Beam's eye" view of quadrupole lens. 26

3.1 Rotation frequency of nonneutral plasma column. 40

3.2 The dimensionless function $\psi(r)$. 44

3.3 The dimensionless function $n(r)/n(0)$. 45

4.1 Circuit for sample and hold module. 51

4.2 The Fermilab ion source test stand beam measurement equipment. 53

4.3 Duoplasmatron ion source. 54

4.4 Emittance probe. 56

4.5 Magnetic Field of the Gabor lens. 61

4.6 Emittance vs. extraction voltage. 63

4.7 Geometry for Abel transform. 64

4.8 Abel inverse of Gaussian input distribution. The circles represent the output of the computer program; the solid line is the calculated inverse. The normalization of f is arbitrary. 68

4.9 Abel inverse of waterbag input distribution. The circles represent the computer calculated inverse, the solid curve is the analytic inverse. 69

4.10 Input x density, Inverted density $f(r)$, electric field, and electrostatic field energy $W(r)$ for 45 keV proton beam. 72

4.11 "Hollow" beam distribution. The units of f are cm^{-3}. 73

4.12 Sample beam distribution at the z_2 position. 74

4.13 Sample beam distribution at the z_3 position. 75

4.14 Field energy W vs. RMS emittance. 77

4.15 Field energy W vs. perveance. The data is fit to the curve $(1.98 \times 10^{-7})/x$ 78

4.16 Nonlinear field energy U (dimensionless) vs. rms beam size in cm. 79

4.17 Noise readings on emittance wires. 81

4.18 Low level readings on emittance wires from an emittance run. . . 83

4.19 RMS emittance vs. fraction of beam removed. 85

Chapter 1

INTRODUCTION

1.1 Introduction

1.1.1 Motivation and Background

This research project began with the goal of developing a new technique for matching a low energy space charge dominated beam into a radio frequency quadrupole accelerator (RFQ). The general problem of the transport of low energy space charge dominated beams is a difficult blend of plasma physics, accelerator physics, and statistical mechanics. The goal of the designer of a low energy beam transport (LEBT) is to transport the beam to the next acceleration section, usually a drift tube linac, while preserving the "quality" of the beam (emittance). A LEBT is the system of focusing elements and field free regions (drifts) between the ion source and the linac. In the ideal case the beam would be transported from the ion source to the RFQ or linac with a negligible emittance growth. In practice there is a rapid emittance growth which occurs within one-quarter of a

plasma period after the beam has left the ion source. [2] So as accelerator designers we must strive to limit this growth of emittance while providing a good "match" of the beam into the RFQ. Lower emittance beams are generally more desirable from the experimenters point of view. For example, when the emittance is lowered, the rate of collisions is increased in a colliding beam accelerator like the Fermilab Tevatron.

A note on units: unless otherwise stated, the units used throughout this paper will be rationalized MKS units. The most common exception to this will be the particle density n, which we tend to express in cm^{-3}. For a general discussion of units, the reader is referred to the appendix of Jackson's book. [19]

Historically the need for intense beams has been driven by experimental physics. In colliding beam experiments the signal of interest is proportional to the intensity of the beam squared, hence the desire to increase the beam intensity. This relationship is expressed mathematically through

$$\mathcal{L} = \frac{\mathrm{fN}^2}{4\pi\sigma_x\sigma_y} \tag{1.1}$$

where $\mathcal{L}$ is the luminosity in $cm^{-2}s^{-1}$, f is the frequency of beam-beam collisions, N is the number of particles in a beam "bunch," and σ_x and σ_y are the transverse spot size of the beam at the collision point. Since $\sigma \propto \varepsilon^{1/2}$, the emittance, $\mathcal{L} \propto \varepsilon^{-1}$.

In the early days of modern physics the experiments were involved with atomic physics. As accelerator physicists learned how to build better accelerators with higher energy beams, the atomic and nuclear physicists examined the atomic and sub-atomic realm at smaller and smaller length scales. Even today physicists at high energy accelerator facilities such as Fermilab and CERN are striving to

examine the fundamental particles of nature at increasingly smaller length scales which correspond to higher beam energies in the accelerators. With the completion of the Superconducting Super Collider (SSC), the highest attainable energy will have reached a new level an order of magnitude larger than the previous highest beam energy, attained in the Tevatron at Fermi National Accelerator laboratory. This growth of energy places a requirement on the emittance of the beams used for high energy physics experiments; since the cross sections for the fundamental processes involved are proportional to E^{-2}, where E is the energy of the interaction, the emittance must also scale like E^{-2} if a given reaction rate is to be maintained.

Lapostolle [24] and Sacherer [37] realized that the emittance growth of a space charge dominated beam is driven by the electrostatic field energy of the beam. Thus it is desirable to neutralize the beam space charge in order to limit emittance growth. One method through which neutralization occurs is in the passing of the beam through the residual gas in a vacuum chamber. The beam particles ionize the gas atoms through collisions. Since the beam is a potential well for charged particles of the opposite sign, neutralization can occur when the particles become trapped in the well. This can also lead to interesting physical phenomena through the beam-plasma interaction.

Another way to neutralize the beam space charge is to provide a compensating charge of the opposite sign to the beam, e.g. a nonneutral plasma. * This is how a Gabor lens neutralizes a proton beam. A nonneutral plasma is a collection of charged particles in a plasma state which does *not* exhibit overall charge

*It should be noted that a neutral plasma can also neutralize the space charge of a beam.

neutrality. A charged particle beam is an example of a nonneutral plasma. The Gabor lens plasma is another example which we shall discuss at length below. In addition to providing neutralization, a Gabor lens is also an azimuthally symmetric focusing device, at least for positively charged beam particles. The focusing strength of a Gabor lens is given by

$$\kappa^2 = -\left(\frac{m\,\omega_p^2}{4T}\right)\left(\frac{Q}{q}\right), \tag{1.2}$$

where κ^2 is the focusing strength squared of the lens in m^{-2}, q and m are the charge and mass of the plasma particles, Q is the charge of the beam particles, $T = mv^2/2$ is the kinetic energy of the beam ions, and $\omega_p = \sqrt{nq^2/\epsilon_0 m}$ is the plasma frequency. The focusing strength is a measure of the ability of the lens to curve the path of the beam particles. For a thin lens, it is equal to the negative inverse of the focal length, thus it has units of inverse length. If we write the equation of motion of the charged particle passing through the lens in the transverse coordinate x, then it is given by

$$x'' + \kappa^2 x = 0. \tag{1.3}$$

The primes denote differentiation with respect to the length coordinate z, which is the axis along which the particle is moving. Note that q and Q are algebraic quantities and that κ is in general a function of z. In order to obtain a positive focusing strength for a Gabor lens the plasma and the beam must have opposite charge, i.e. "opposite charges attract."

Since it supplies a compensating charge to the unneutralized ion beam, provides a strong focus, and exhibits azimuthal symmetry, a Gabor lens seems to be a prime candidate for a LEBT focusing device. Whether or not this is so

must be determined by practical experience. It was found in the course of this thesis that a Gabor lens is not an ideal focusing element for a LEBT. This will be discussed below in detail. At the time of this writing, magnetic solenoid or electrostatic lenses must be considered more appropriate for solving the problem of low energy beam transport. The only practical application of a Gabor lens to date of which this author is aware has been in an ion microprobe beam line with a very small current of the order of 1 pA or less. [27] The beam in this experiment had a negligible space charge. On the other hand in the LEBT regime the beam density is nearly comparable to that of the plasma and hence is able to perturb it or perhaps even excite an instability.

A large step forward in the theoretical understanding of emittance growth in space charge dominated beams was taken with the previously mentioned papers of Lapostolle and Sacherer. Additional insight was found by Hoffman, [18], Wangler [41], and Anderson [2]. These authors presented a theory in which electrostatic field energy was the driving force behind emittance growth. A differential equation was discovered which relates the change of the emittance with z, the axial length coordinate, to changes in the field energy: [41]

$$\frac{d\varepsilon^2}{dz} = -\frac{KX^2}{2}\frac{d}{dz}\left(\frac{U}{W_0}\right) \tag{1.4}$$

where K is now the generalized perveance (to be defined), X is twice the RMS width of the beam, U is the "nonlinear field energy," (to be defined) and $W_0 = (eN)^2/16\pi\varepsilon_0$ is a constant determined by the line density N of the beam. W_0 is physically equivalent to the field energy contained within the boundaries of the beam. This equation was first written in a different form by Lapostolle in his 1970 paper. [24] At first glance the equation appears simple to solve, until one realizes

that $X = X(z)$. The evolution of X is determined by the envelope equation

$$\frac{d^2X}{dz^2} + \kappa^2 X = \frac{\varepsilon^2}{X^3} + \frac{K}{X} \tag{1.5}$$

in which κ is again the focusing strength, and K is the "generalized perveance." [25] The envelope equation contains the emittance ε. Thus the equations are coupled. In practice it is no easier to solve this pair of equations then it is to solve the Vlasov equation from which they are derived. Fortunately, an experiment involving a real beam is relatively simple to set up and observe, so that insight into the dynamics of emittance growth can be gained from actually observing a beam.

1.1.2 Summary of the Thesis

First, a note on units. We will use rationalized MKS units throughout, unless stated otherwise. The common exception to this will be that the particle density n is usually expressed in cm^{-3}.

The focus of all the research presented in this thesis is the area of low energy beam transport. It has been stated that there are strong motivations for preserving the emittance of a beam in an accelerator at all stages of the acceleration process. Early on, in February of 1987, it was thought that a Gabor lens showed some promise as a means of doing this. A Gabor lens has azimuthal symmetry, which greatly simplifies the design of the beam transport, since the entrance conditions ("acceptance") of an RFQ are also azimuthally symmetric. Using quadrupole type lenses complicates the design.

Our first Gabor lens was constructed in 1988. The solenoid was rather large (for a Gabor lens), being 2 feet in length. It was designed to carry a current of

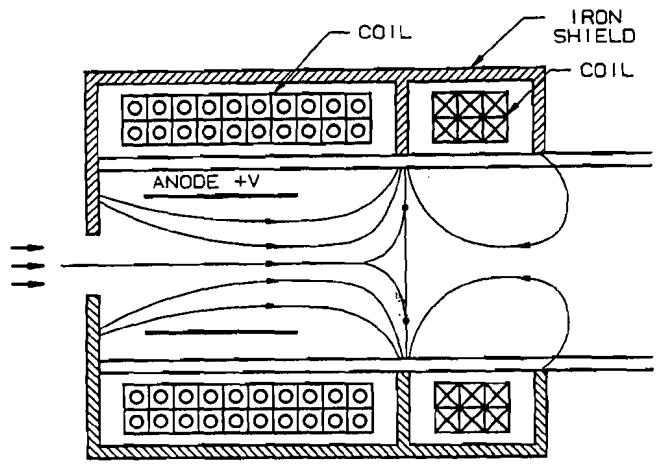

Figure 1.1: Fermilab Gabor lens.

up to 200 Amps with water cooled conductor wires. We later found that it was not necessary to use this large a solenoid to trap the Gabor lens plasma. At the time our first lens was constructed it was not understood what the relationship is between the plasma density and the magnetic field strength. The *Brillouin limit* gives the maximum nonneutral plasma density that can be contained by a magnetic field B_0:

$$n = \frac{2\varepsilon_0 B^2}{m}. \tag{1.6}$$

Using this equation, one finds that to trap an electron plasma with $n \sim 10^{16} m^{-3}$ a magnetic field of strength at least equal to 7.1×10^{-3} Tesla $= 71$ Gauss is needed. In laboratory experiments one finds that the density n is well below the Brillouin limit. In the experiments done at Fermilab, n for the Gabor lens plasma was typically .07 of the limiting value. Thus to trap the electron plasma with $n \sim 10^{16} m^{-3}$ one would use a field of approximately 300 Gauss ($\sim 71/\sqrt{.07}$).

What this means is that it is possible to use a simple air cooled solenoid magnet to provide the magnetic field for the Gabor lens.

Another problem with using the large solenoid magnet was discovered early on in the experiment. The ion source being used was a proton source of the duoplasmatron type. This source depends on a magnetic field for its operation. It was discovered that the magnetic field of the large solenoid was perturbing the field of the duoplasmatron and making it unstable, which was quite visible on an oscilloscope trace of the current pulse from the duoplasmatron. Having learned from our mistakes, we decided to construct a second Gabor lens with improved features.

The second Gabor lens was designed with an air cooled primary coil and a smaller secondary coil in opposition to the primary. See figure (1.1). This was so that a cusp could be created in the magnetic field on the axis of the lens. The reason for doing this is simple - it gives the plasma greater stability. We will discuss this stability issue below. There are also increased losses, but these are not a problem since the lens is run in a discharge mode which continually replenishes the plasma density.

We found that the Gabor lens did provide a focus of the proton beam. However that focus was not as sharp as we had hoped. In order to match a low energy proton beam into an RFQ, a very sharp focus must be obtained just before the entrance into the RFQ. The transverse beam dimensions must be on the order of 200 μm. The Gabor lens focal spot was never observed to be this small, being on the order of 1 cm in size.

A program of emittance measurements was undertaken to try to understand

what the transformation of the beam is in traversing the Gabor lens. This involved a series of emittance runs both upstream and downstream of the Gabor lens. Knowing the beam phase space before and after the lens one can then infer what the effect of the lens on the beam is.

As we have mentioned a very important problem in low energy beam transport is to try and limit the emittance growth experienced by a beam as it traverses a LEBT. Therefore the LEBT designer must have an understanding of the dynamics of emittance growth in low energy space charge dominated beams.

Many hours of computer time have been spent by others "verifying" with particle in cell codes that the relations expressed by equations (1.4) and (1.5) are correct. We decided to perform a simple experiment which would test these relations. An experimental apparatus was available in the Fermilab ion source test stand. We undertook an investigation of the evolution of the distribution function of the beam and the emittance as the beam propagated through a short distance on the test stand. This was just a drift space, no focusing elements were involved. The emittance of the beam was measured at several locations in z, the beam direction, to see if some understanding of the dynamics of emittance growth could be obtained through direct measurement.

We found that the experimental results were in fairly good agreement with the theory. The emittance grew over a distance of 7 cm by a factor of ~ 2. This is roughly equal to 1/4 of a plasma wavelength for the test stand proton beam.

New Results

There were essentially three new results from this thesis research.

We found that a Gabor lens was not capable, with current technology, of focusing a negative ion beam. This is a theoretical result. It may be possible some day to maintain a nonneutral positron plasma in a Gabor lens in order to effectively focus a negative ion beam, but it is not possible today.

We used an Abel Inversion procedure applied to a proton beam charge distribution to calculate the electrostatic field energy of the beam. This quantity is of great importance in the theory of emittance growth in space charge dominated beams.

Finally, we observed emittance growth on a scale length which was small compared to the plasma wavelength of the beam. This is the distance the beam travels in an internal plasma oscillation.

1.2 The Problem of Low-Energy Beam Transport

1.2.1 The Need For Intense Beams

We have mentioned that the transport of intense low-energy ion beams is an outstanding problem of accelerator physics today. Experimentalists at accelerators and heavy-ion fusion facilities need more intense beams to do the experiments which are at the forefront of science in their fields. There is always an interaction point where physically interesting collisions and reactions occur and these reactions are more plentiful at high intensity. Therefore, at existing accelerator facilities such as Fermilab and CERN, physicists are always pushing to reach

higher energies and intensities. One is therefore confronted with the question: what limits the intensity of an accelerator? Liouville's theorem places a constraint on the final beam emittance (ordinarily it cannot be less than the initial emittance[†]), and hence the possible luminosity at the interaction point. We shall provide a precise definition of emittance below; for now we remark that emittance is related to the volume occupied by the beam particles in phase space. The maximum possible luminosity is ultimately constrained by the emittance of the beam leaving the ion source in a proton accelerator. Thus we seek to always preserve the emittance at every step of the acceleration process.

At a large high energy proton accelerator facility such as Fermilab, there are several accelerators arranged in series to accelerate the beam to the final energy. We are concerned with the very beginning of the acceleration process where the beam is created in an ion source and then transported to the input of a linear accelerator. The transport of the proton beam in this low-energy regime is a crucial part of the overall acceleration process. The emittance will grow in the low energy beam transport (LEBT) by a factor of two or three. We are interested in minimizing this emittance growth in the LEBT for many reasons; as we have already mentioned the preservation of a low emittance can lead to increased luminosity in collider experiments being performed with the accelerator. Low emittance beams are less likely to scrape the beam pipe in the upstream portions of the accelerator because of their small transverse dimensions. The current state of the art in linac design is to use a radio frequency quadrupole (RFQ) accelerator to accelerate the beam in the energy regime from several tens of kilovolts to 2.5

[†]The emittance of a beam can be decreased via beam cooling techniques.

MeV. The optical matching of the beam into the entrance of an RFQ requires great precision and a very strong focusing of the beam. This places constraints on the LEBT, as we shall see.

Some emittance growth is inevitable in any accelerator or beam transport line. Nonlinearities due to the focusing fields and the beam self fields lead to amplitude dependent oscillation frequencies of the beam particles and the dilution of the phase space density of the beam. By carefully designing accelerator components, we seek to minimize the emittance growth which inevitably occurs. In order to understand the methods by which we hope to limit emittance, we shall have to investigate the theoretical physics of space charge dominated beams.

1.2.2 Beam Optics and the Definition of Matching.

First a note on coordinate systems. The standard arrangement in accelerator physics is to define a beam axis which is usually taken to be the z axis of a cartesian coordinate system, with x, y, and z forming a right handed coordinate system. In the literature s is often used instead of z. In general, the path the beam takes is curved, however, we will only be concerned with linear systems in what follows.

The purpose of a LEBT is to prepare the beam for acceleration in a linear accelerator (linac). Given a linac, transport line, or circular accelerator, we must decide what the proper beam parameters are to inject into it. We will consider the case of a uniform transport line ($k =$ const.), with a monochromatic (p_z the same for all particles) beam, for simplicity. The results can be extended to more complicated situations. In this case the individual particle motions are described

by a harmonic oscillator equation. The particles trajectories are sinusoids in z. Equation (1.5) describes the evolution of the rms beam envelope X in the transport line. The generalized perveance K is defined by

$$K = \frac{2I}{I_0(\gamma\beta)^3}, \; I_0 = \frac{4\pi\varepsilon_0 mc^3}{q}. \tag{1.7}$$

I_0 has the units of current and is numerically about 3.1×10^7 Amps for protons. We define the matched beam as having $X'' = 0$. Inserting this into (1.5) and solving for X we have, using a to denote the solution,

$$a = \sqrt{\frac{K}{2\kappa^2} + \sqrt{\left(\frac{K}{2\kappa^2}\right)^2 + \left(\frac{\varepsilon}{\kappa}\right)^2}}. \tag{1.8}$$

If we have a beam with negligible current then $K \sim 0$; we obtain

$$a_0 = \sqrt{\frac{\varepsilon}{\kappa}} \tag{1.9}$$

where a_0 is the matched beam envelope size in the absence of current. In terms of this result (1.8) becomes

$$a = a_0\sqrt{\frac{K}{2\kappa^2 a_0^2} + \sqrt{\left(\frac{K}{2\kappa^2 a_0^2}\right)^2 + 1}}. \tag{1.10}$$

If, however, we have a strongly space charge dominated beam then the emittance term in the envelope equation is neglected and we find

$$a_1 = \frac{\sqrt{K}}{\kappa}. \tag{1.11}$$

for the size of the beam. Using the definitions of a_0 and a_1 we can rewrite equation (1.10) to read

$$\mathrm{a} = \sqrt{\frac{\mathrm{a}_1^2}{2} + \sqrt{\frac{\mathrm{a}_1^4}{4} + \mathrm{a}_0^4}} \tag{1.12}$$

In this form it is easy to see how the two limits are obtained. Equation (1.12) tells us that as the current increases from zero ($a_1 = 0$) then the matched beam size for a given transport line increases. When the matched size is equal to the size of the beam pipe we have reached the maximum current which can be transported through the pipe.

If the beam is not matched into the focusing structure, then the envelope of the beam will oscillate as z increases. It is easy to substitute $X = a + \delta$, where $\delta \ll a$, into (1.5) and Taylor expand, keeping only lowest order terms, to obtain

$$\delta'' + 2\left(\kappa^2 + \frac{\varepsilon^2}{a^4}\right)\delta = 0 \tag{1.13}$$

which shows that the envelope oscillations are simple harmonic with wavelength

$$\lambda = \frac{2\pi}{\sqrt{2\left(\kappa^2 + \varepsilon^2/a^4\right)}}. \tag{1.14}$$

These envelope oscillations have an adverse affect for space charge dominated beams. They cause emittance growth. Since real beams are not uniform, the oscillation frequencies of the particles in the beam are amplitude dependent, hence the phase space is "diluted" when the envelope oscillates.

If the transport channel is non-uniform, e.g. a system of alternating quadrupole lenses, then the matched beam envelope is no longer independent of z. The matched beam is now defined as that beam which has an envelope X with the same periodicity as the focusing structure. Note that this is not inconsistent with the definition of matching for a uniform focusing channel. The period for the uniform channel is infinite.

In order to find the matched solution one must solve (1.5) with the appropriate initial conditions. A mismatched beam will exhibit envelope oscillations with a

periodicity not equal to that of the focusing structure. In addition, in a periodic structure, the envelope oscillations can develop into an instability, which causes emittance growth. The instability can develop whenever the wavelength of the zero current solution to (1.5) becomes less than four periods of the focusing structure. [35]

1.2.3 Emittance Growth of Space-Charge Dominated Beams.

We will provide here a brief review of the theory of emittance growth in space charge dominated beams. We start with the equations discovered by Kapchinskii and Vladimirskii in 1959. [21] What Kapchinskii and Vladimirskii found was that if the distribution of the beam particles in the transverse phase space x, x', y, y' was given as

$$\mathrm{f(x,y,x',y')} = \delta\left[\mathrm{F_0} - \left(\frac{\mathrm{x}^2}{\mathrm{a}^2} + \frac{\mathrm{y}^2}{\mathrm{b}^2} + \frac{\mathrm{a}^2\mathrm{x}'^2}{\varepsilon_{\mathrm{x}}^2} + \frac{\mathrm{b}^2\mathrm{y}'^2}{\varepsilon_{\mathrm{y}}^2}\right)\right] \tag{1.15}$$

where F_0 is a constant related to the constants of the motion for the transverse single particle motion, [21] and δ is the Dirac delta function, then the semiaxes of the (elliptical) beam obey the following equations, known as the "K-V" equations:

$$a'' + \kappa_x a = \frac{2K}{a+b} + \frac{\varepsilon_x^2}{a^3} \tag{1.16}$$

$$b'' + \kappa_y b = \frac{2K}{a+b} + \frac{\varepsilon_y^2}{b^3} \tag{1.17}$$

where κ represents external focusing forces, K is the perveance, ε the emittance, and a and b are the dimensions of the beam envelope.

The K-V equations are important because they provide a useful approximation to the behavior of real beams which are not axially symmetric. If the "smooth approximation" is made then they can be solved analytically for some important cases involving beams in realistic transport systems. It is worth noting that the envelope equation (1.5) is a special case of the K-V equations with $a = b = X$.

With the K-V equations in hand, it is possible to calculate beam envelopes for space charge dominated beams only if the emittance, which appears on the right hand sides of the equations, is a given function of z, and the beam distribution function is a K-V distribution. However, this is an ideal case suited only for the theoretical study of beam dynamics. A useful approximation for quick calculation is to assume a constant emittance and an axisymmetric beam.

Progress in the area of space charge dominated beam transport was made with two papers published in 1970 by Lapostolle and Sacherer. [24, 37] Both showed the importance of an rms formulation for calculating the evolution in time of the properties of a space charge dominated beam. In computer simulations the rms emittance [‡] of a beam transported through a uniform focusing channel was found to oscillate with an overall increase in the emittance. This behavior is sketched in figure (1.2).

Lapostolle identified two distinct types of oscillations which led to emittance growth in space charge dominated beams: oscillations of the beam envelope and

[‡]The rms emittance of a beam is given by the formula

$$\varepsilon = \frac{4}{p_z}\sqrt{\langle x^2\rangle \langle p_x^2\rangle - \langle x p_x\rangle^2} \tag{1.18}$$

where p_z is the average momentum of the particles in the direction of motion of the beam; x and p_x are a transverse displacement and momentum, respectively.

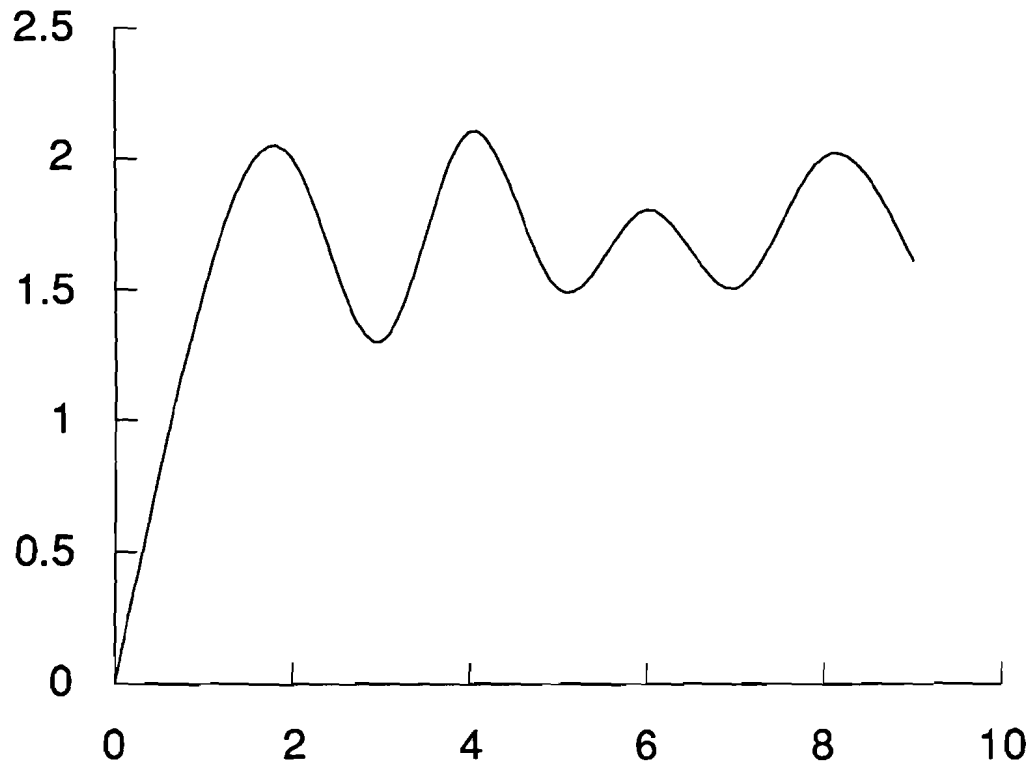

Figure 1.2: Evolution of the beam emittance in a uniform focusing channel.

oscillations of the charge density in the beam.

Sacherer showed that the K-V equations were not restricted to the case of a beam with a K-V distribution function. In fact, they could be applied to any beam in which the charge was distributed with elliptical symmetry, i.e., the distribution function could be written as

$$f = f\left(\frac{x^2}{a^2} + \frac{y^2}{b^2}\right), \tag{1.19}$$

if the beam boundary and emittance are specified by rms values. However, this does not get around the problem that the time dependence of the rms emittance must be known beforehand in order to solve for the envelope of the beam.

Further progress in the theoretical understanding of emittance growth came from the work of Wangler, Hoffman, and others in the mid 1980's. These researchers discovered an equation relating emittance growth to electrostatic field energy in a beam. Starting with the Vlasov-Maxwell equations one can arrive at equation (1.4) for an axially symmetric beam. [41, 18] In (1.4) $U = W - W_u$ where W is the electrostatic field energy per unit length, given by

$$W = \pi\varepsilon_0 \int_0^\infty r E_r^2 dr. \tag{1.20}$$

Physically, W_u is the electrostatic field energy per unit length of a uniform beam with the same current and energy as the real beam. It is given by

$$W_u = W_0 (1 + 4\ln(b/X)), \; b \geq X, \tag{1.21}$$

where b is the radius of the (assumed present) beam pipe and $X = 2\sqrt{\overline{x^2}}$ is twice the width of the beam. We see that $W_0 = (eN)^2/16\pi\varepsilon_0$ is the field energy within the uniform beam, with the logarithmic term giving the contribution from the

field outside of the beam. The magnetic field energy of the beam is negligible for non-relativistic beams and is not considered here.

About a year later, Anderson published a paper which showed that for certain initial beam distributions it is possible to analytically calculate the evolution of the beam envelope and the emittance simultaneously. [2] He found that there was an "explosive" growth in the emittance which occurred over a distance of one quarter of a plasma wavelength as a "cold" beam began to propagate in a focusing channel. In this context, cold means that the transverse kinetic energy of the beam distribution is small compared to the energy contained within the electrostatic field of the beam.

Thus we have arrived at a picture in which emittance growth is driven by the excess or nonlinear space charge field energy in the beam, excess being defined as greater than that of the equivalent uniform beam. It can be shown that the quantity $W - W_u$ is positive definite. [18] The related quantity $(W - W_u)/W_0$ is essentially a function of the shape of the charge distribution, being zero for a perfectly uniform beam and non-zero otherwise. The space charge dominated beam will evolve to an equilibrium state in which the density in the center of the beam is uniform. As the beam evolves toward a uniform density the emittance increases and W decreases. This conversion of space-charge field energy to emittance is really a conversion of potential to kinetic energy with a corresponding increase in the entropy of the beam. Thus it is possible to understand emittance growth as being related to the second law of thermodynamics. It can be shown that the entropy of a beam is given by a simple formula involving the emittance. [26]

1.2.4 Experimental Techniques Used with Space-Charge Dominated Beams

There are, of course, a plethora of techniques for creating, transporting, and accelerating space charge dominated beams. We shall only discuss those which pertain to the goals of this thesis, namely transport of low energy proton beams. From this viewpoint, then, there are two main elements to proton beam transport: neutralization and focusing. The type of focusing element used has a large effect on the neutralization, so the two topics are related.

Neutralization is a very important and complex phenomenon in low energy beam transport. When a beam encounters a low pressure gas in the vacuum vessel through which it is propagating, ion-electron pairs are created in collisions. This process can create a plasma which then interacts with the beam. Particles with the same sign of charge as the beam are repelled from the beam, while oppositely charged particles are attracted. If the beam current is DC or changing over a time scale which is sufficiently long it is possible for an equilibrium state to form in which particles are lost at the same rate at which they are created. For a gas of density n, beam particles moving at velocity v, and ionization cross-section σ, the neutralization time τ is given by the simple expression

$$\tau = (n\sigma v)^{-1} . \tag{1.22}$$

If the ion source is pulsed with a pulse length of the same order of magnitude as τ, then the neutralization of the beam will always be changing, which makes matching the beam into a focusing structure difficult. Unfortunately for the densities and velocities typically encountered with low energy proton beams this

is often the case. For example, the proton source on the Fermilab ion source test stand is often run with gas density $n \simeq 10^{11} cm^{-3}$ and speed $v \simeq 8 \times 10^{-3} c$. If we take the cross section to be the "billiard ball" cross section of a gas atom $10^{-15} - 10^{-16} cm^2$, then we find $\tau \simeq 4$ - $40 \mu s$. The pulse length used is typically $100\,\mu s$ hence the neutralization state of the beam is changing during a significant part of the pulse length. This makes it difficult to keep the beam matched into downstream structures.

However, if the beam pulse is long enough then the initial part can be discarded and the latter part used when the beam has stabilized. This has a disadvantage in that the useful life of the ion source is wasted since part of each pulse is not used.

The type of lens used has a large effect on the neutralization. If a conventional electrostatic lens is used, e.g. an electrostatic quadrupole, then any low-energy ion or electrons created in beam gas collisions will be immediately swept out of the beam by the electric field in the vicinity of the lens. Conversely for a magnetic lens, trapping of the low-energy ions and electrons can occur as they spiral around the magnetic field lines. Thus magnetic lenses must be used if beam induced neutralization is to occur in the vicinity of the lens.

There is another way to neutralize the beam. If the beam encounters a non-neutral plasma with the opposite sign of charge then immediate neutralization can occur on the time scale of a plasma period. [10] In our experiments there was no observation of time dependent neutralization for the beam passing through a Gabor lens, which contained a nonneutral plasma. The other extreme is to use electrostatic lenses and prevent neutralization completely. There is some increase

in emittance growth when this approach is taken since the field of the beam is what drives the growth, as we have seen.

1.3 Lenses used in low-energy beam transport

We can classify the lenses used in low energy beam transport into two types: azimuthally symmetric (axisymmetric) lenses and lenses which are not axisymmetric, for example a quadrupole lens. We can further divide these two classes into two types each: magnetostatic and electric lenses. Of the symmetric lenses, we will consider the Gabor lens, the magnetic solenoid, and the electrostatic lens. For the non-symmetric lenses, there is the electric and magnetic quadrupole and the helical quadrupole.

1.3.1 Azimuthally symmetric lenses

The Solenoid Lens

The solenoid is a particularly simple and robust means of providing focusing to a low energy proton beam. In the form usually used for beam transport, it consists of a coil of wire wrapped by an iron yoke to concentrate magnetic flux in the region of the beam.

The focal length of a solenoid is given by the expression

$$\frac{1}{f} = \int \left(\frac{qB}{2mv}\right)^2 dz \tag{1.23}$$

where f is the focal length. [25] The integral is taken along the axis of the solenoid. Since the focusing is second order in the field strength and charge, the focusing

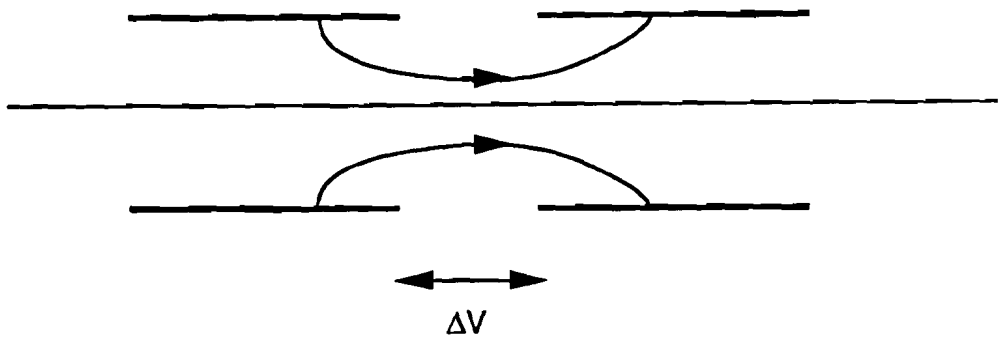

Figure 1.3: Electrostatic cylinder lens.

is always positive, i.e. beam particles are deflected towards the axis in traversing the lens. Also because the beam particles follow helical paths in the solenoid the beam undergoes a net rotation in passing through. However, no net angular momentum is imparted to the beam.

Neutralization effects can be significant for an intense beam propagating through a solenoid. Charged particles formed in the lens move slowly in the direction perpendicular to the field. The trapping of charged particles in the region of the beam increases the effective focusing force of the lens and can significantly enhance the amount of current which can be transported through the lens. [36] It takes time for neutralization to occur. The focusing is changing during this time, which can have adverse consequences.

The Electrostatic Cylinder Lens

The azimuthally symmetric electrostatic lens comes in a number of configurations. The simplest consists of two coaxial cylinders with a bias voltage applied between them. The focusing is due to the fringe fields at the entrance and exit of the lens

and the fact that the beam particles undergo acceleration in the lens. As with the solenoid, the focusing is second order in the field strength. The expression for the focal length is given approximately by

$$\frac{1}{f} = \frac{3}{16}\left(\frac{\Phi_1}{\Phi_2}\right)^{1/4} \int \left(\frac{\Phi'}{\Phi}\right)^2 dz \tag{1.24}$$

where Φ_1 is the potential of the tube at the lens entrance, Φ_2 that of the exit tube, and Φ is the electrostatic potential.

The electrostatic cylinder lens suffers from spherical aberration, as does the solenoid. Spherical aberration limits the attainable minimum spot size which can be achieved with a lens,[17] so it is an important consideration for lenses that will be used to match into RFQs. An RFQ requires a very sharp beam focus at its input. Spot size requirements of a millimeter in size or less are typical.

Neutralization effects do not exist in an electrostatic lens. Any free ions or electrons created in collisions with beam particles are immediately swept out of the lens by the electric field. This can be a great advantage in designing a LEBT using electrostatic lenses. However, emittance growth is greater than the growth that would occur in a neutralized beam precisely because the electric field of the beam is not neutralized.

The Gabor Lens

It is possible to obtain a focusing which varies with the first power of the field by placing current or charge in the path of the beam. The Gabor lens is an example of the latter. [15] It works by producing a stable cloud of electrons in the lens. If the cloud is perfectly uniform in density, the fields will vary linearly with radius

and the lens will have very good focusing properties. The actual form of the equilibrium plasma density distribution will be derived below.

The focal length of a Gabor lens is given by

$$\frac{1}{f} = \kappa \sin(\kappa L) \tag{1.25}$$

where $\kappa = -(m\omega_p^2/4T)(Q/q)$ is the focusing strength, $T = mv^2/2$ is the kinetic energy of the beam ions, Q is the charge of the beam ions, q is the charge of the plasma particles, and $\omega_p = \sqrt{nq^2/\epsilon_0 m}$ is the plasma frequency.

The Gabor lens has some very desirable properties for LEBT. The beam is neutralized while passing through the lens, so emittance growth is limited. The focusing is strong. It is not clear if high beam currents can be transported through the lens. If the density of beam particles is not much less than the density of the nonneutral plasma in the lens, then beam-plasma instabilities may develop, limiting the focusing precision of the lens. The lens must be able to sustain a plasma for long periods of time if it is to be used in an accelerator operation environment.

1.3.2 Nonsymmetric Lenses

The discussion of nonsymmetric lenses will be brief. There is only one which is used in LEBT, the quadrupole lens. The focusing properties of electric and magnetic quadrupoles are identical.

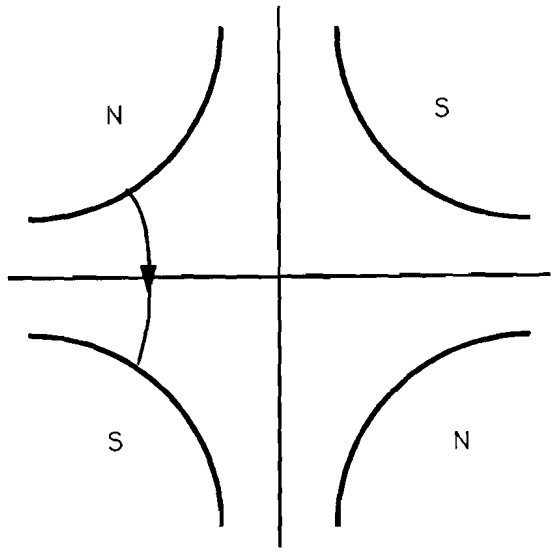

Figure 1.4: "Beam's eye" view of quadrupole lens.

Quadrupole Lenses

By employing a lens geometry which has two symmetry planes, it is possible to obtain a lens in which the focusing is first order and linear. The quadrupole lens is focusing in one plane while defocusing in the other, perpendicular, plane. For example, if we take the beam axis to be the z axis of cartesian coordinate system, then if the quadrupole focuses particles moving in the xz plane it will defocus particles traveling in the yz plane. It must be used in a more complex configuration to construct a LEBT, using the lenses in an alternating arrangement to obtain a focusing array. This is dependent on the fact that a pair of lenses of equal strength, one focusing, the other defocusing, has a net focusing effect. This phenomenon is used to great advantage in an alternating gradient synchrotron. [9] In order to obtain the equivalent of a thick lens which is focusing in both planes,

three quadrupoles in a symmetric triplet arrangement must be used. Quadrupole LEBTs require more lenses to take a given beam and match it into a given structure. Electrostatic quadrupoles are totally immune to neutralization effects, magnetic quadrupoles nearly so.

The focal length of a magnetic quadrupole lens is given by the expression

$$\frac{1}{f} = k \sin(kL) \tag{1.26}$$

where

$$k^2 = \frac{q}{p_z}\frac{\partial B_y}{\partial x} = \frac{q}{p_z}\frac{\partial B_x}{\partial y} \tag{1.27}$$

and L is the length of the quadrupole and $p_z = mv_z$. For an electrostatic quadrupole the same expression holds for $1/f$ with

$$k^2 = \frac{q}{mv^2}\frac{\partial E_y}{\partial x} = \frac{q}{mv^2}\frac{\partial E_x}{\partial y}. \tag{1.28}$$

Chapter 2

PHYSICS OF BEAMS WITH SPACE CHARGE

2.1 Characteristics of Space Charge Dominated Beams

2.1.1 Distribution Functions and Phase Space

In this thesis we shall refer many times to beams of charged particles. Therefore it is necessary to begin by defining a beam. Following Lawson [25] we shall define a beam as a distribution of charged particles, roughly cylindrical in shape, which are moving with their velocity vectors approximately parallel to a line called the beam axis. In all the situations which we shall discuss, the angles between the velocity vectors and the beam axis are small enough that the paraxial approximation may be used.

Consider a system composed of N identical charged particles. This could be a plasma for example. Classically the state of the system is completely specified by the 6N coordinates and momenta of the particles. The systems we will be dealing with have large numbers of particles, greater than 10^{10}, hence any attempt to specify all the coordinates and momenta of the particles is futile. From a statistical viewpoint this is analogous to specifying the N particle distribution function

$$f = f(\mathbf{q}_1, \cdots, \mathbf{q}_N; \mathbf{p}_1, \cdots, \mathbf{p}_N; t).$$

The interpretation of this function f is that the probability that the particles in the system have coordinates $\mathbf{q}_1, \cdots, \mathbf{q}_N$ and momenta $\mathbf{p}_1, \cdots, \mathbf{p}_N$ in the ranges $\mathbf{dq}_1, \cdots, \mathbf{dq}_N$ and $\mathbf{dp}_1, \cdots, \mathbf{dp}_N$ at the time t is given by the expression

$$f(\mathbf{q}_1, \cdots, \mathbf{q}_N; \mathbf{p}_1, \cdots, \mathbf{p}_N; t) d\mathbf{q}_1, \cdots, d\mathbf{q}_N; d\mathbf{p}_1, \cdots, d\mathbf{p}_N.$$

The function f satisfies the following equation:

$$\frac{\partial f}{\partial t} + \sum_{i=1}^{3N} \dot{q}_i \frac{\partial f}{\partial q_i} + \dot{p}_i \frac{\partial f}{\partial p_i} = 0. \tag{2.1}$$

This result is known as Liouville's theorem [30] and it has profound implications for the behavior of a distribution of particles. It is of fundamental importance in statistical mechanics. Although the N particle description is complete, it is quite intractable for a system with a large number of particles.

We shall instead describe the system with a reduced one particle distribution function $f = f(\mathbf{q}, \mathbf{p}, \mathbf{t})$, where $\mathbf{q}$ and $\mathbf{p}$ are the generalized coordinate and momentum vector of a particle in the Hamiltonian sense. The one particle distribution function is formally related to the N particle distribution function by

an integral:

$$f(\mathbf{q}_1, \mathbf{p}_1, t) = \int F d\mathbf{q}_2, \cdots, d\mathbf{q}_N d\mathbf{p}_2, \cdots, d\mathbf{p}_N \tag{2.2}$$

The physical significance of f is that fd^3qd^3p is the number of particles in the system in the phase-space volume element d^3qd^3p located at $(\mathbf{q}, \mathbf{p})$. The function f is normalized so that $\int fd^3qd^3p = N$, the number of particles in the system. The density of particles in the lab is n. If the plasma approximation is valid, [22] the distribution function f and the density n satisfy the Vlasov-Maxwell equations:

$$n(\mathbf{q}) = \int fd^3p \tag{2.3}$$

$$\frac{\partial f}{\partial t} + \frac{1}{m}\mathbf{p} \cdot \nabla_{\mathbf{q}}\mathbf{f} + \mathbf{q}\left(\mathbf{E} + \frac{\mathbf{v} \times \mathbf{B}}{\mathbf{c}}\right) \cdot \nabla_{\mathbf{p}}\mathbf{f} = \mathbf{0} \tag{2.4}$$

$$\nabla_q \cdot \mathbf{E} = \frac{qn}{\varepsilon_0} \tag{2.5}$$

$$\nabla_q \cdot \mathbf{B} = 0 \tag{2.6}$$

$$\nabla_q \times \mathbf{B} = \mu_0 \mathbf{J} + \frac{\partial \mathbf{E}}{\partial \mathbf{t}} \tag{2.7}$$

$$\nabla_q \times \mathbf{E} + \frac{\partial \mathbf{B}}{\partial \mathbf{t}} = \mathbf{0} \tag{2.8}$$

where $\nabla_{\mathbf{q}}$ denotes the gradient operation with respect to coordinate q, $\nabla_{\mathbf{p}}$ with respect to momentum p. $\mathbf{E}$ and $\mathbf{B}$ are the electric and magnetic field vectors, $\mathbf{J}$ is the current density, and ε_0 and μ_0 are the usual electromagnetic constants. [19] The distribution function and the fields are coupled through this set of equations.

If the beam current is independent of time or if the variations in the beam current occur over a much longer time than the period of plasma oscillations of the beam we can write equation (2.4) as

$$\frac{\partial f_\perp}{\partial t} + \frac{1}{m}\left(p_x \frac{\partial f_\perp}{\partial x} + p_y \frac{\partial f_\perp}{\partial y}\right) + F_x \frac{\partial f_\perp}{\partial p_x} + F_y \frac{\partial f_\perp}{\partial p_y} = 0 \tag{2.9}$$

where $f_\perp = f_\perp(x, y, p_x, p_y, t)$ and F_x and F_y are the x and y components of the electromagnetic self force

$$\mathbf{F} = q\left(\mathbf{E} + \frac{\mathbf{v} \times \mathbf{B}}{c}\right). \tag{2.10}$$

Formally this "transverse" distribution function is obtained from the full six dimensional function $f = f(\mathbf{q}, \mathbf{p}, \mathbf{t})$ by integrating over all values of z and p_z:$f_\perp(x, p_x, y, p_y, t) = \int f(\mathbf{q}, \mathbf{p}, \mathbf{t})\, dz dp_z$. This equation is useful if we have some knowledge of the analytical form of the distribution function. If we wish to simulate the time evolution of the beam distribution function then we can do so with a particle in cell (PIC) code.

2.1.2 Standard Beam Parameters

We will attempt to follow as closely as possible the notational conventions of Lawson.[25] We shall describe the beam by specifying a number of parameters. A complete description would include the current, energy, type of particle and the distribution function of the beam. In practice one is lucky to know the current, energy, and one of the second moments of the transverse distribution function of the beam. Any spread in the energy value of the beam is neglected. When we speak of the energy it should be understood that we mean the kinetic energy $T = (1/2)mv^2$ of the particles, equal to the total accelerating potential they have fallen through. Since the beams dealt with are non-relativistic ($v/c < 10^{-2}$), the non-relativistic formula for kinetic energy can be used.

We shall choose a cartesian coordinate system whose z-axis coincides with the beam axis. We then choose the x-axis to lie in a horizontal plane and the y-axis to

be vertically upward such that x, y,and z form a right-handed coordinate system. If the beam distribution is azimuthally symmetric then a cylindrical coordinate system r, θ,and z will be used.

One way of specifying some of the properties of the beam distribution is by using three parameters which we shall refer to as the Courant-Snyder parameters $\alpha_{x,y}$, $\beta_{x,y}$, and $\gamma_{x,y}$. [12]. The x, y notation indicates that the Courant-Snyder parameters are defined for either transverse plane x or y. In a linear accelerator or a beam transport line, the Courant-Snyder parameters are intimately associated with the beam, and their values must be specified at some point in order for them to be defined. In a circular accelerator like a synchrotron the Courant-Snyder parameters are determined by the magnetic field structure of the accelerator itself in the absence of any beam. We shall be discussing linear beam transport, hence we will be using them in the first sense in which they are associated with the beam. They may be determined experimentally from measurements of the beam phase space. If one measures the transverse distribution of the beam in the x, p_x plane then the Courant-Snyder parameters can be defined by the following set of equations:

$$\alpha_x = -\frac{4\langle xp_x\rangle}{\varepsilon_x p_z}, \beta_x = \frac{4\langle x^2\rangle}{\varepsilon_x}, \gamma_x = \frac{4\langle p_x^2\rangle}{\varepsilon_x p_z^2} \tag{2.11}$$

where the $\langle\rangle$ denote averages over the beam distribution and

$$\varepsilon_x = \frac{4}{p_z}\sqrt{\langle x^2\rangle\langle p_x^2\rangle - \langle xp_x\rangle^2} \tag{2.12}$$

is our definition of the *RMS emittance*. [1, 29, 24] It is sufficient for our purpose here to define the Courant-Snyder parameters and the emittance in this way. It

follows from (2.11) and (2.12) that

$$\gamma_x \beta_x - \alpha_x^2 = 1. \tag{2.13}$$

2.1.3 Liouville's Theorem and the Emittance

The theory we are presenting is statistical in nature. Since Liouville's theorem is fundamental to statistical mechanics it is not surprising that it has a fundamental role in the theory of space charge dominated beams. We present here a brief definition of the concept of emittance, which is vital to the theory of space charge dominated beams. At Fermi National Accelerator Laboratory there is a standard definition for the beam at high energy, depending on the beam width from flying wire measurements and the value of the beta function of the magnet lattice at the point where the measurement is taken. [32] This is due to the fact that there is no way to measure the angular width of the beam at energies greater than 10 MeV. Unfortunately the other high energy physics laboratories do not use the same definition of emittance as Fermilab * so that caution must be exercised when comparing numbers from different experiments. For low energy beams the situation is much better. There is a commonly accepted definition of emittance which is in widespread use. It can be accurately measured in a reproducible fashion, and is a good indicator of the nature of the particle beam. For a detailed discussion of emittance the reader is referred to the excellent monograph of Lejeuene and Aubert [29] A good discussion can also be found in Lawson's book. [25]

*When fitting beam width measurements, the full emittance is defined as contained within two standard deviations at CERN and $\sqrt{6}$ standard dev. at Fermilab. But even within the laboratories there is variation in the definition used.

In order to understand emittance one must try to understand Liouville's theorem, equation (2.1). The state of the system at a given time is a single point in the $6N$ dimensional phase space of the coordinates and momenta of the particles in the system. The N particle distribution function specifies the probability density of the state of the system in this space. As the system evolves in time the system point traces out a path in phase space. Only one path can pass through any given point. This is because Hamilton's equations [16]

$$\dot{p}_i = -\frac{\partial H}{\partial q_i} \tag{2.14}$$

$$\dot{q}_i = \frac{\partial H}{\partial p_i} \tag{2.15}$$

are first order differential equations. The subscript i ranges from 1 to N so that there are $2N$ equations total. The function

$$H = H\left(q_{1x}, \ldots, q_{zN}, p_{1x}, \ldots, p_{zN}, t\right) \tag{2.16}$$

is the Hamiltonian function of the system, which may be derived from the Lagrangian function. The only important point here is that the equations of motion can be put in the form of Hamilton's equations. Since the equations are first order in the time, the path of the system point is uniquely determined by the initial conditions of the motion. Now consider an ensemble of systems all with different initial conditions of their coordinates and momenta at some instant of time t. As these systems evolve in time their system points trace out paths which do not cross in phase space. Thus a group of system points contained within a boundary remains within the boundary as the system evolves in time. If we define a density function $f(q_i, p_i, t)$ of system points in phase space then it will obey a continuity

equation (the number of systems is a constant). By combining Hamilton's equations with this continuity equation we can arrive at (2.1) [30] which states that the density of system points in the neighborhood of a particular system point does not change with time. One can consider this ensemble of points as a sort of fluid. Liouville's theorem says that the fluid flow is incompressible.

Liouville's theorem is true in general only in the $6N$ dimensional phase space of the coordinates and momenta of all N particles. If the particles interact, it is not in general possible to simplify this result and recast it in terms of the one particle distribution function. However, if the interaction is collective and the plasma approximation holds [22], then (2.1) becomes the Vlasov equation.

Consider now the reduced one particle distribution function f, which lives in the six dimensional space of Hamiltonian coordinates and momenta. If there are interparticle forces, then in general Liouville's theorem must be modified. The simplest approach is to approximate the interaction of the charged particles of the system with the smooth electric field of all the charges. The Vlasov-Maxwell equations are then used to solve for the properties of the system. If the effects of short-range collisional forces are to be included in the theory then the Boltzmann equation must be used. [8]

How, then, is Liouville's theorem connected with the emittance? Consider again a system for which Liouville's theorem holds for the one particle distribution function. An emittance ε can be defined to be the "area" enclosed by the particles in the two dimensional phase space of one of the coordinates and its conjugate momentum. Assume that the motion is uncoupled, i.e., the Hamiltonian separates into three parts each of which depends on one of the coordinates and

its conjugate momentum. Liouville's theorem says that the emittance is constant in time:

$$\frac{d\varepsilon}{dt} = 0. \tag{2.17}$$

It is worth pointing out that the "area" occupied by a collection of particles must be carefully defined in a theoretical sense. In classical mechanics a particle is represented by an infinitesimal point in phase space. Thus it seems the total area occupied by any collection of particles is zero. One imagines a boundary enclosing the collection of particles in phase space which delimits the volume, but it is not clear how to choose the boundary. It is possible to choose the boundary by a statistical process; this is what the rms emittance does. The rms emittance does not necessarily obey Liouville's theorem. Its time rate of change is covered by (1.4) if the beam is azimuthally symmetric.

In practice, when the emittance is measured, what is usually obtained is an intensity signal $I(x, x')$, where $x' = p_x/p_z$. The boundary of the distribution is defined as a particular intensity level. The emittance is taken to be the two dimensional area contained within this curve in the x, x' plane, and it has units of length.

Chapter 3

PHYSICS OF GABOR LENSES

A Gabor lens, figure (1.1), is a device which traps a nonneutral plasma column. The other distinguishing characteristic of the lens besides nonneutrality is the azimuthal symmetry. Radial confinement is provided by a solenoidal magnetic field, axial confinement by the electric field of one or more electrodes. Since the plasma is nonneutral, it creates an electrostatic field which will focus a positively charged particle beam. We will discuss some of the plasma physics of the Gabor lens in this chapter.

3.1 Nonneutral Plasma Physics

Nonneutral* plasma physics is a subfield of plasma physics which has seen much increasing activity in the last several years. [11] In 1989 the Nobel prize in physics

*This is the spelling used by most authors in the field. The AIP hyphenates it (non-neutral) in their journals and conference proceedings.

was awarded to physicists doing research in nonneutral plasma physics. A nonneutral plasma is a collection of charged particles which does *not* exhibit overall charge neutrality. There is an excess of one charge species relative to the other. Examples occur in ion and electron traps, intense relativistic electron beams, klystrons, free electron lasers, low energy ion beams, etc. Nonneutral plasmas are characterized by intense electrostatic self fields due to the nonneutrality of the system. In all cases of interest they are also magnetized. It is the magnetic field which provides the restoring force necessary to keep the system in equilibrium. An unneutralized cloud of charge tends to disperse itself because of the electrostatic repulsion exhibited by like charges.

The choice of the magnetic field configuration is very important and must be made with care. The stability of any magnetized plasma including nonneutral plasma can be shown to depend in a general fashion on the curvature of the magnetic field lines. [22] If the field lines curve into the plasma then it is stable and vice versa.

3.1.1 The Brillouin Limit

We will now discuss an important fundamental limit on the attainable density of a plasma in a Gabor lens or cylindrical ion-trap type geometry. This limit was first calculated by Brillouin in 1945. [6] Consider a distribution of particles all of the same mass m and charge species q which is symmetric about the z axis in a cylindrical coordinate system r, θ, z. There are no charges of the opposite sign to q in the system, so it is *nonneutral*. We consider the plasma to have much greater extent in the z direction than in radius, with a uniform line density so

that we can ignore variations of the charge density in z, $\partial n/\partial z = 0$. There is a uniform magnetic field in the $-\hat{\mathbf{z}}$ direction $\mathbf{B} = -B\hat{\mathbf{z}}$.

The fluid equation of motion of the cold plasma with zero pressure gradient and no collisions is given by

$$mn\left[\frac{\partial \mathbf{v}}{\partial t} + (\mathbf{v}\cdot\nabla)\,\mathbf{v}\right] = nq\left[\mathbf{E} + \mathbf{v}\times\mathbf{B}\right]. \tag{3.1}$$

We also have from Gauss's law $\nabla\cdot\mathbf{E} = \rho/\varepsilon_0$ that the electric field in the plasma column is $E_r = (nq/\varepsilon_0)r$. We look for a steady state solution of (3.1) and Gauss's law with $\partial/\partial t = \partial/\partial\theta = 0$. Combining the two we obtain the force balance equation:

$$m\frac{V_\theta^2}{r} = -\frac{1}{2}\left(\frac{nq^2}{\varepsilon_0}\right)r + qBV_\theta. \tag{3.2}$$

The θ component of (3.1) vanishes identically with the stated assumptions. Equation (3.2) has a simple interpretation. The term on the left is the centripetal acceleration of a small fluid element. The first term on the right comes from the outward electrostatic self-force of the nonneutral plasma and the second term on the right represents the inward magnetic force which binds the system. This is a quadratic equation for $\Omega = V_\theta/r$. Solving for Ω we find

$$\Omega = \left(\frac{\omega_c}{2}\right)\left[1 \pm \left(1 - \frac{2\omega_p^2}{\omega_c^2}\right)^{1/2}\right], \tag{3.3}$$

where $\omega_p^2 = nq^2/\varepsilon_0 m$ is the plasma frequency and $\omega_c = qB/m$ is the cyclotron frequency of a particle in the magnetic field. Equation (3.3) is plotted in figure (3.1). Since the rotation frequency is independent of r, equation (3.3) describes a rigid rotation of the plasma as a whole. We note that for each value of $2\omega_p^2/\omega_c^2$ there are two possible rotation frequencies given by the intersection of a vertical line with the upper and lower branches of the parabolic curve, *except* when

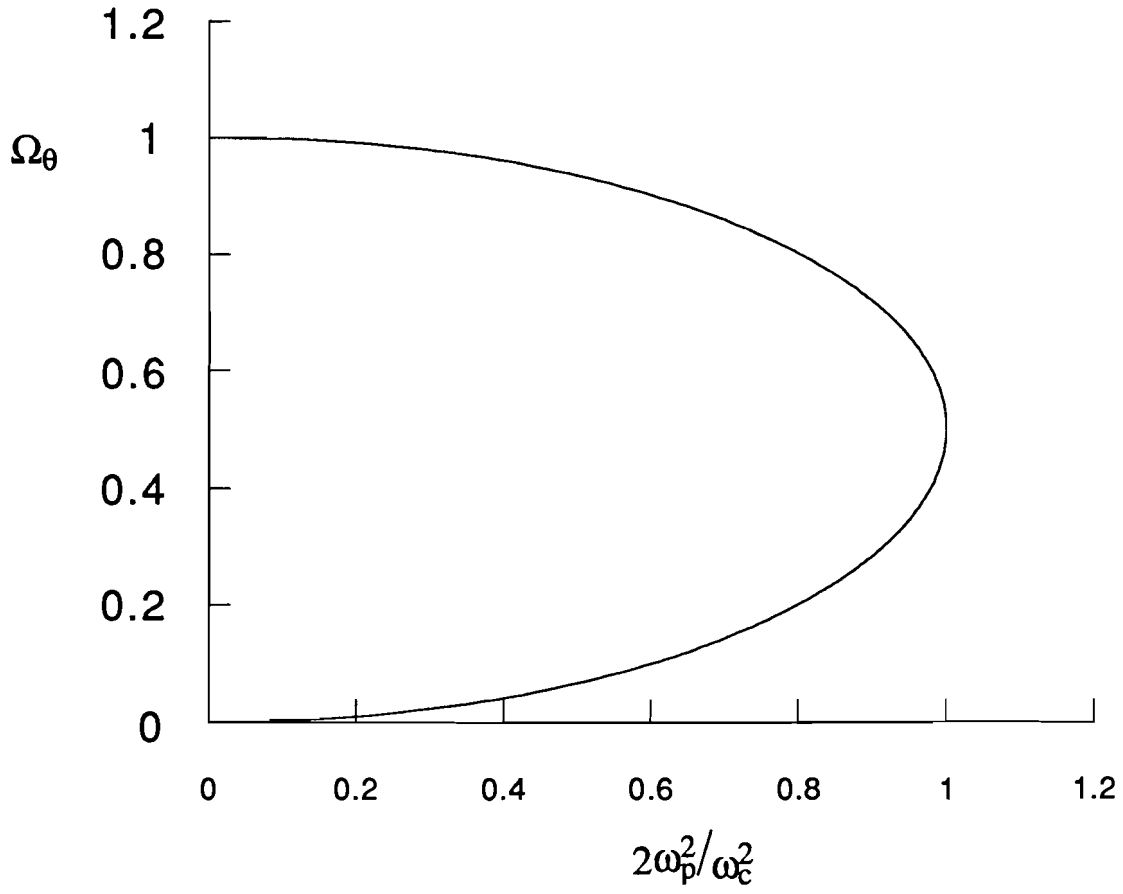

Figure 3.1: Rotation frequency of nonneutral plasma column.

$2\omega_p^2/\omega_c^2 = 1$, or $\Omega = \omega_c/2$. This is known as the *Brillouin limit* or *Brillouin flow*, which was mentioned above. We rewrite it here for convenience. In terms of the plasma density n we have

$$n = \frac{2\varepsilon_0 B^2}{m} \propto \frac{B^2}{m} \tag{3.4}$$

at the limit.

It is interesting to see what condition if any results from applying the same assumptions (azimuthal symmetry, time independence, and infinite length of the column) to the single particle equation of motion for a plasma particle. The equation of motion of a plasma particle is

$$m\ddot{\mathbf{r}} = q\left(\mathbf{E} + \mathbf{v} \times \mathbf{B}\right) \tag{3.5}$$

which we can rewrite as

$$\ddot{\mathbf{r}} = \frac{1}{2}\omega_p^2 \mathbf{r} + \omega_c \dot{\mathbf{r}} \times \hat{\mathbf{z}}. \tag{3.6}$$

Now transform to a coordinate system rotating with angular velocity Ω_r using

$$x' = x\cos\Omega_r t + y\sin\Omega_r t \tag{3.7}$$

$$y' = -x\sin\Omega_r t + y\cos\Omega_r t. \tag{3.8}$$

In the rotating coordinate system the equation of motion (now written in component form) is, with $\mathbf{B} = -B\hat{\mathbf{z}}$ as before,

$$\ddot{x}' = \left(\Omega_r^2 - \omega_c\Omega_r + \frac{1}{2}\omega_p^2\right) x' - \left(\omega_c - 2\Omega_r\right)\dot{y}' \tag{3.9}$$

$$\ddot{y}' = \left(\Omega_r^2 - \omega_c\Omega_r + \frac{1}{2}\omega_p^2\right) y' + \left(\omega_c - 2\Omega_r\right)\dot{x}'. \tag{3.10}$$

Now choose Ω_r to be the solution (3.3) so that the first terms on the right side of (3.10) will vanish leaving

$$\ddot{x}' = -\left(\omega_c - 2\Omega_r\right)\dot{y}' \tag{3.11}$$

$$\ddot{y}' = (\omega_c - 2\Omega_r)\,\dot{x}'. \tag{3.12}$$

This pair of equations is familiar from the problem of charged particle motion in a static, homogeneous magnetic field. The plasma particles are found to be executing circular orbits in the rotating frame with the frequency $\omega_c - 2\Omega_r$. When Ω_r equals $\omega_c/2$ then the particles are at rest in the rotating frame and when Ω_r vanishes then the particles are describing cyclotron orbits. Thus the same limits apply to Ω_r as apply to Ω in the fluid case. This is reasonable since the fluid velocity represents an average velocity of all the particles in the plasma. If we average over many cyclotron orbit periods then the average motion is represented by the motion of the rotating frame.

3.1.2 Finite Temperature Equilibrium of a Nonneutral Plasma Column

We shall now investigate the effect of a finite temperature on the equilibrium of the plasma column. This requires the insertion of a temperature term into equation 3.1. The modified equation now reads [8]

$$mn\left[\frac{\partial \mathbf{v}}{\partial \mathbf{t}} + (\mathbf{v}\cdot\nabla)\,\mathbf{v}\right] = nq\,(\mathbf{E} + \mathbf{v}\times\mathbf{B}) - \nabla p. \tag{3.13}$$

We will use the same coordinate system as in the previous section. We are searching for an equilibrium solution of (3.13) and Gauss' law $\nabla\cdot\mathbf{E} = \mathbf{nq}/\varepsilon_0$. Writing (3.13) out we have with $\partial/\partial t = 0$

$$(\mathbf{v}\cdot\nabla)\,\mathbf{v} = \frac{q}{m}\mathbf{E} - \omega_c\,(\mathbf{v}\times\hat{\mathbf{z}}) - \frac{kT}{m}\nabla\psi \tag{3.14}$$

where ψ is defined as

$$\psi = \ln(n/n_0).$$

Now we shall make what may seem like a restrictive assumption. We are looking for an equilibrium solution of (3.13) and Gauss' law which is a description of the state of the system. There is a theorem from statistical mechanics which states that if a system is in thermodynamic equilibrium then its macroscopic motion must consist of a uniform translation and/or rotation.[23] We shall therefore assume that our system is undergoing uniform rotation so that we may write $\mathbf{v} = v_\theta \hat{\theta}$. Using this equation we have that

$$(\mathbf{v} \cdot \nabla)\mathbf{v} = \left(\omega \frac{\partial}{\partial \theta}\right) \omega r \hat{\theta} = -\omega^2 r \hat{\mathbf{r}}.$$

Inserting this into (3.14) we obtain

$$-\omega^2 r \hat{\mathbf{r}} = \frac{q}{m}\mathbf{E} - \omega_c (\mathbf{v} \times \hat{\mathbf{z}}) - \frac{kT}{m}\nabla\psi. \tag{3.15}$$

Now take the divergence of this equation to obtain, after some rearrangement

$$\nabla^2\psi = \frac{2m\omega}{kT}(\omega - \omega_c) + \frac{m\omega_p^2}{kT}e^\psi \tag{3.16}$$

or, since $\partial/\partial z = \partial/\partial\theta = 0$,

$$(\rho\psi')' = \rho\left(g + e^\psi\right) \tag{3.17}$$

where $g = 2\omega(\omega - \omega_c)/\omega_p^2$, $\rho = r/\lambda_d$, and λ_d is the *Debye length* [22, 8] defined by the equation

$$\lambda_d = \sqrt{\frac{kT}{m\omega_p^2}}. \tag{3.18}$$

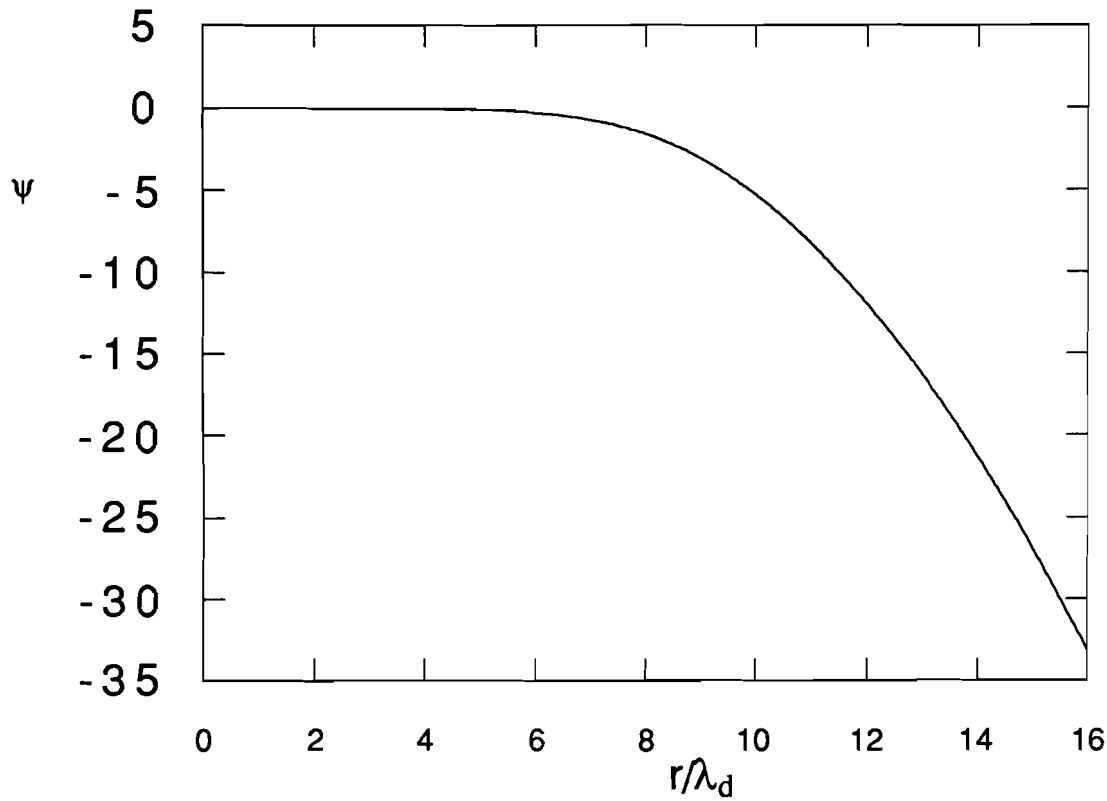

Figure 3.2: The dimensionless function $\psi(r)$.

The $'$ denotes differentiation with respect to ρ . This is a singular, nonlinear differential equation. It is not known to have a general solution in terms of analytic functions. Fortunately, equation (3.17) can be accurately integrated with a Runge-Kutta integration routine on a computer. The correct initial value problem is to solve (3.17) with the initial conditions $\psi(0) = \psi'(0) = 0$. A graph of the solution for ψ is shown in figure (3.2) for $g = 0.005$. If we now take the exponential of ψ the the function $n(r)$ is obtained. This is plotted in figure (3.3). We see the general behavior of the function - it is flat from the middle of the

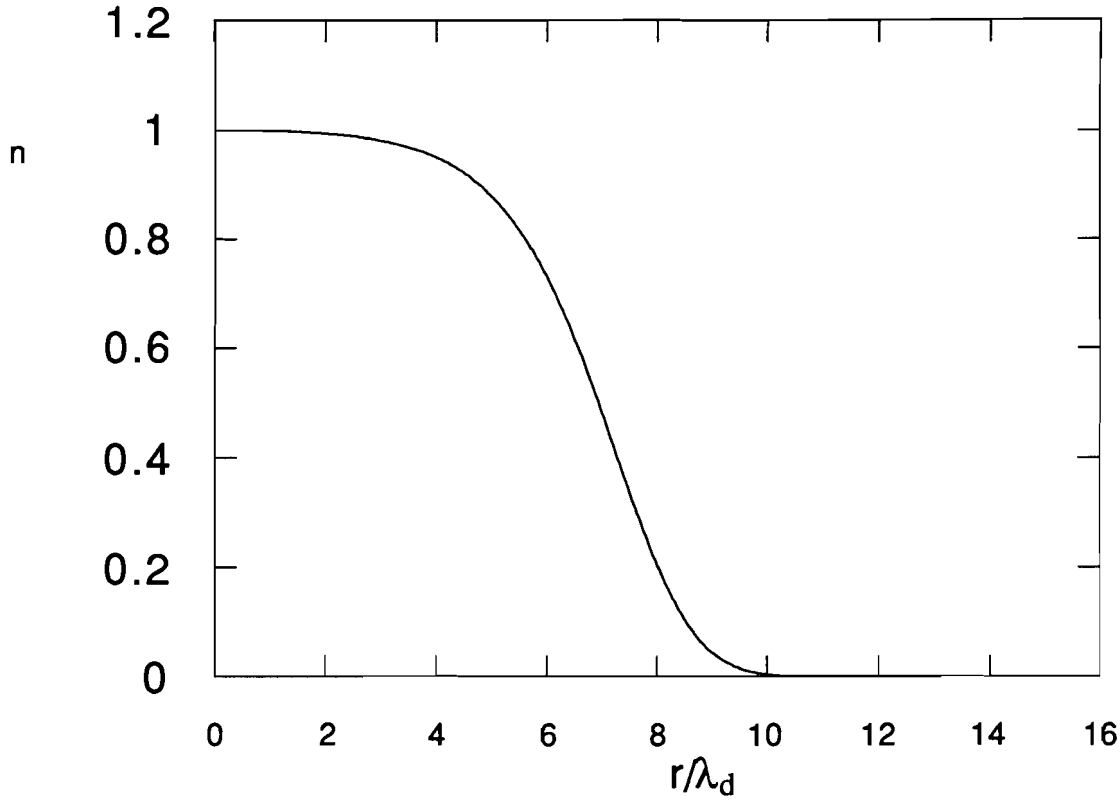

Figure 3.3: The dimensionless function $n(r)/n(0)$.

column to several Debye lengths from the z-axis. The column width depends on the parameter g. As g decreases, the width of the column increases. Outside the flat region in the center of the column there is a gentle falloff to zero density with a scale length of λ_d.

3.1.3 On the Difficulty of Focusing Negative Ion Beams with a Gabor Lens

Because of the fact that the charge to mass ratio of the electron is larger than that of any other easily generated charged species seen in laboratory nonneutral plasmas, the Gabor lens has an interesting property. It is only useful for focusing beams containing positively charged species. This asymmetry arises because of the need to confine the nonneutral plasma with a solenoidal magnet. In order to focus a given beam we need a certain electric field strength. This yields a focal length. The electric field strength is determined by the central (nonneutral) plasma density in the lens. In addition we must have the plasma density in the lens much greater than the density of the beam, in order that the beam space charge is neutralized. We must construct a magnetic field strong enough to contain this density in the Gabor lens. We recall that the maximum possible density in the center of the lens is given by $n = 2\varepsilon_0 B^2/m$. This is the Brillouin limit. Now we must inquire into what density is necessary in the Gabor lens to focus the beam. Let us take the H^- beam from the Fermilab magnetron source as an example. Typical beam densities are $\sim 10^8\, cm^{-3}$. Assume the density of the Gabor lens plasma to be $\gtrsim 10^9\, cm^{-3}$. If we plug a density of of $n = 10^9\, cm^{-3}$, and a lens length L of $10cm$ (this should approximate our Gabor lens; the measured

density was in the $10^8 - 10^9 cm^{-3}$ range, while the electrode length was 10 cm.) into the focal length equation (1.25), then, assuming we are focusing 30 keV protons, we find that $f \simeq 9cm$.

The nonneutral plasma particles must be positively charged to focus the negative beam. One could imagine forming a proton plasma from hydrogen gas. However the plasma particles are now 1836 times more massive then they are for an electron plasma. This means that we need a large magnetic field, as given by the Brillouin limit. We should also take into account the fact that laboratory plasmas of this type are usually well below the Brillouin limit when in equilibrium. In the Fermilab Gabor lens we obtained a plasma with $2\,\omega_p^2/\omega_c^2 \simeq 7 \times 10^{-2}$. For $n = 10^9\, cm^{-3}$ we find that $B \sim 1$ Tesla. This is a strong solenoid magnet. So strong that the focusing effect of the magnet is just as great as that of the nonneutral plasma, making the combined focusing effect too large. In addition, it would be necessary to shield any nearby ion source from the field of the beam. The magnet would be large and costly to construct. This is to be contrasted with an electron Gabor lens which can be made with a simple air core magnet with a central field of $\simeq 200G$.

3.2 Focusing properties

3.2.1 The fields of the Nonneutral Column

Because the charge density ρ of the plasma column contained in the Gabor lens is non-zero, there is an *electrostatic* field in the region of the plasma given by

Gauss's law,

$$\nabla \cdot \mathbf{E} = \frac{\rho}{\varepsilon_0} \tag{3.19}$$

where $\mathbf{E}$ is the electric field vector and ε_0 is the "permittivity of free space," a constant. For a plasma column in which the charge density is independent of z we obtain the elementary result:

$$E_r = \begin{cases} \left(\frac{m}{2q}\right)\omega_p^2 r & 0 \leq r \leq R \\ \left(\frac{m}{2q}\right)\omega_p^2 \left(\frac{R^2}{r}\right) & R \leq r \end{cases} \tag{3.20}$$

where $\omega_p = \sqrt{nq^2/\epsilon_0 m}$ is the plasma frequency. This electric field leads to the equivalent thin-lens focal length [33] given by (1.25) for beam particles moving within the body of the plasma.

In general, the density will not be completely uniform and the electric field will have a z component. This means treating the column as having a finite length. Numerical methods must be used to solve the Vlasov-Maxwell equations in all but the simplest cases. With certain assumptions, it is possible to solve for the electrostatic potential. [34]

One could also use detailed knowledge of the charge density ρ in order to solve (3.19) (numerically) for the electric field. Since there was no measuring capability for the plasma density as a function of r and z within the lens, we were not able to do this. Given that the plasma density is nearly uniform in the body of the plasma, it is a good approximation to treat the lens as a simple thick lens, much like a thick glass lens used in a pair of binoculars, e.g, so such an exercise would only be of academic interest.

Chapter 4

EXPERIMENTAL RESULTS

4.1 Experimental Setup

4.1.1 Data Acquisition Electronics and Software

The data acquisition hardware consisted of a Fermilab linac console [38], a multiple channel sample and hold amplifier board, and a Fermilab "D0 Rack Monitor Module (RMM)." [14] The digital output of the RMM was sent over an MIL-1553 data bus to a token ring interface card housed in a VME crate. The data was then sent over a token ring network to a Sun Microsystems 4/260c computer where it was stored and analyzed. The Sun console was used to examine the data values from the experiment in real time and to debug the emittance measurement apparatus. The functions of the other equipment will be explained below.

The software which controlled the data acquisition was developed on the Sun by several people. It is a mixture of C, C++, and unix shell scripts (the shell is the command line interface for unix and a programming language in its own

right).

A C++ program ("meas_emit") was used to actually control the experiment and acquire the data. There were two separate programs used as "front ends" to meas_emit. One program ("emit-sun") employed a graphical interface and could only run on the Sun graphics console. Most of the data was taken with a unix shell script ("measit") which could be run from any ascii terminal. This was important since the only terminal in the lab was an ascii terminal.

For each emittance run a separate file was created on disk which contained all the raw data associated with the run. We felt it was important to save the raw data to disk. Any manipulation of the data (smoothing, noise removal) was then done in the analysis program without alteration of the original data files.

Multiple Channel Sample and Hold Module

In order to do the analog to digital conversion of the output signals from the experiment, a multiple channel sample and hold circuit was devised. The basic circuit of the the sample and hold module (SHM) was quite simple (figure 4.1). The analog input signal is fed into a Precision Monolithics OP37ez operational amplifier. With the external resistors used in the circuit the gain is 200. The output pin of the op amp is connected to the input of a Harris ha-5320-5 sample and hold amplifier. Since there is a 50 Ω resistor between the op amp input and ground, the output signal was proportional to the current from the wires. The acquisition time of the ha-5320-5 chips is 1μs. That is, the output of the module follows the input until the control voltage goes high, at which point the output is "clamped" within one μs. All the sample and hold modules are controlled by

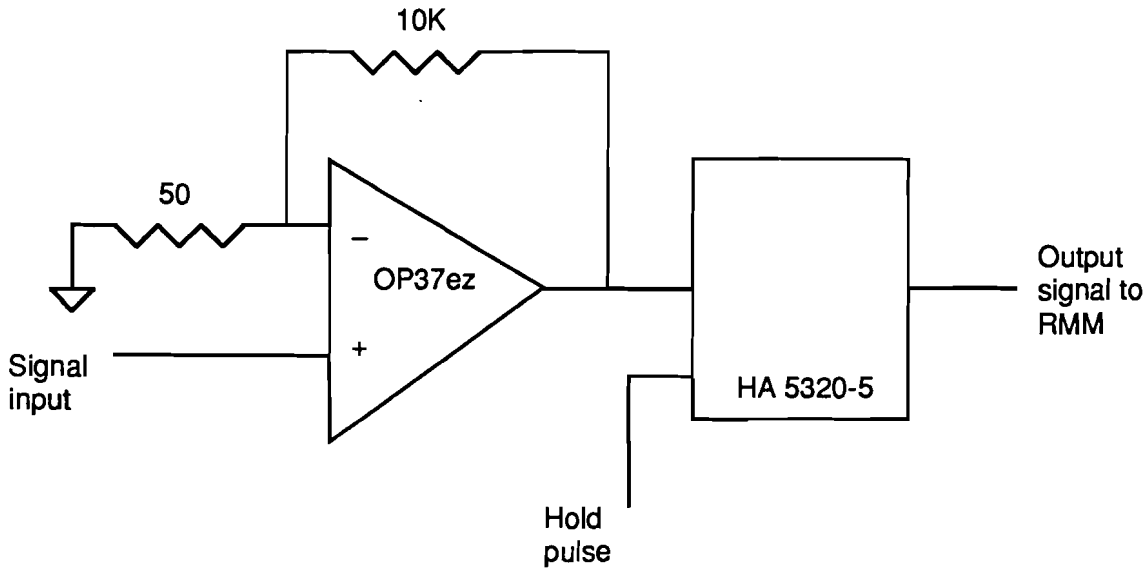

Figure 4.1: Circuit for sample and hold module.

a single hold signal which is buffered out to all the chips through a buffer circuit on the same board. The timing of the hold signal could be varied over the entire length of the beam pulse, which was 90 μs in length. In all of the emittance measurements, the hold signal arrived 50 μs after the start of the beam pulse. We found no significant time variation of the emittance over the length of the beam pulse.

Thirty-six of these circuits were placed in parallel on a single circuit board to provide simultaneous sample and hold capability for the signals from the emittance probe. With fifty signals for the emittance wires, as well as current and high voltage read back, two boards were constructed to provide enough data capacity.

D0 Rack monitor module

The RMM is used to do the analog to digital conversion (A/D) in the experiment. This is a general purpose monitoring module that was designed for monitoring data in the D0 collider detector at Fermilab. It provides 64 channels of A/D conversion with 8 output channels, and four words of digital I/O. The RMM uses an MIL 1553 data bus to communicate with an IEEE 802.5 Token Ring interface card that was developed at Fermilab. The MIL 1553 is a multiplexed, 1 MHz data bus that operates over a shielded, twisted pair cable. In the jargon of MIL 1553, the RMM is a "remote terminal" that is being controlled from a token ring device. Both devices can and do reside within a single VME bus crate. The VME is a standard data bus that is used in many applications in experimental physics.

4.1.2 Ion Source Test Stand and Duoplasmatron

The Fermilab ion source test stand is a general purpose tool for the testing of ion sources and low energy beam transport devices. It has the capability to run with both H^+ (proton) and H^- beams. The Gabor lens (which was discussed previously) is not useful for focusing negative ion beams, and the emittance growth of the beam does not depend on the sign of the beam space charge (if neutralization effects are not important). Hence proton beams were used to do the experiment.

A schematic drawing of the ion source test stand experiment is shown in figure (4.2). Vacuum was provided by a turbo molecular pump with a pumping speed of 450 liter/s. A typical vacuum with the duoplasmatron running was $\sim 10^{-5}$ torr. There was a large ion pump on the test stand but it was not used

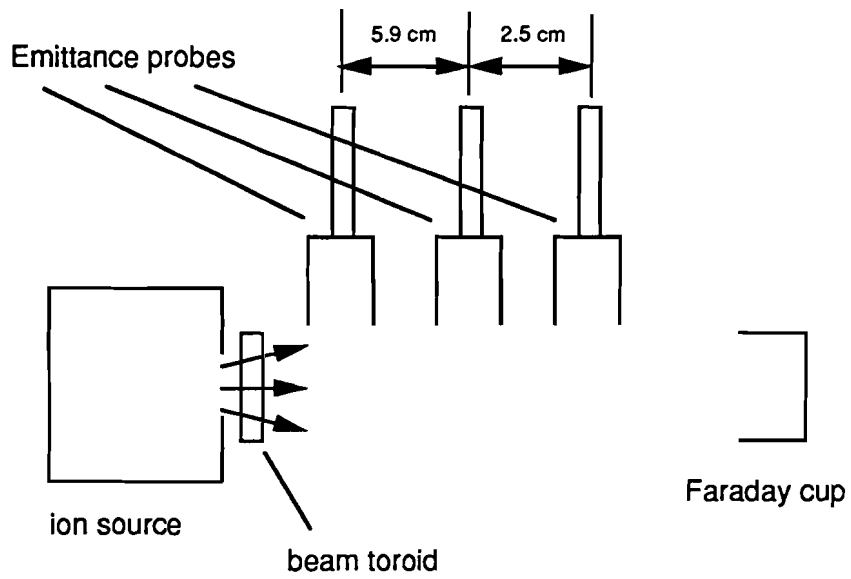

Figure 4.2: The Fermilab ion source test stand beam measurement equipment.

because of difficulties with its operation.

The duoplasmatron is a design that is more than thirty years old. [13] These ion sources were used for operation in the early days of Fermilab. An H^- source is used currently. One of the old Fermilab duoplasmatrons was used for the emittance growth experiment. This particular source is based on a MURA design. A schematic diagram of the ion source is shown in figure 4.3. The apparatus is very nearly azimuthally symmetric, except for the cathode filament. Hydrogen gas is fed into the rear of the source through a gas leak valve. The gas is heated and ionized by the filament, which has a direct current flowing through it. With a voltage of several hundred volts between the filament and the anode, an arc discharge is generated in the gas in the chamber. In the region of the intermediate electrode (IE), a plasma sheath is formed with a corresponding increase in the

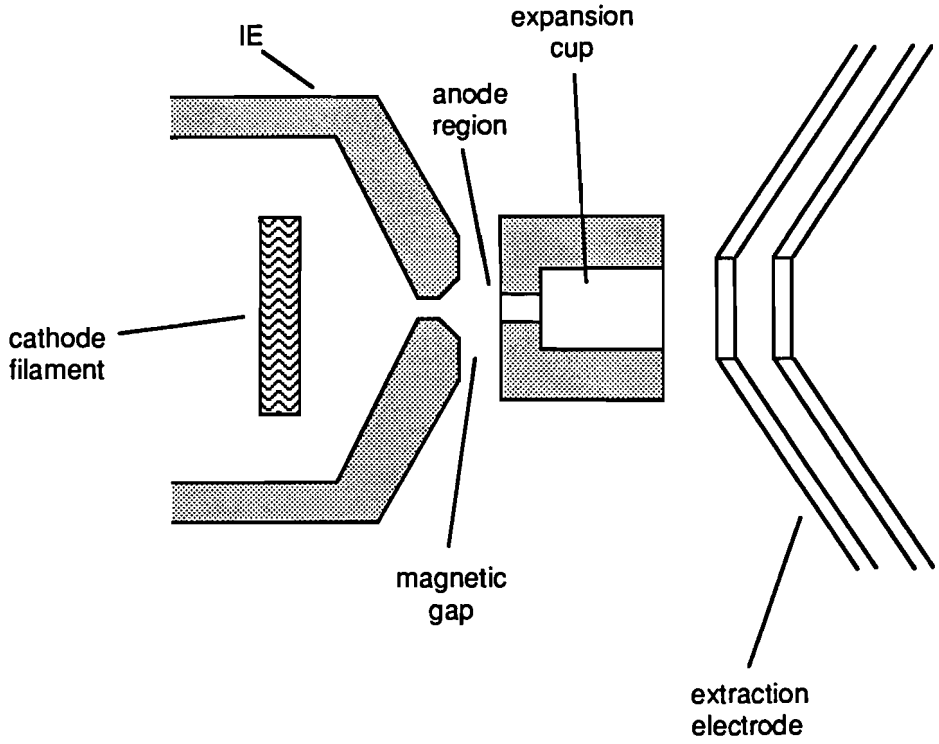

Figure 4.3: Duoplasmatron ion source.

potential on the symmetry axis. There is a strong magnetic field on the order of several kilogauss in the gap between IE and the anode, which are opposite magnetic poles. Because of the strong magnetic field, only the most energetic electrons can traverse this gap into the anode region. Ionization in the second discharge in the expansion cup is due entirely to collisions between these energetic electrons and neutral gas atoms. Another sheath is formed between the second discharge and the extraction electrode, which is biased negatively with respect to the anode. Ions extracted through this second sheath form the beam.

In our experiment, the filament to anode voltage is pulsed with a duty factor of 0.13 % (90 μs, 15 Hz). The output current of the source shows a rise time of $\sim 5\mu$s, then the current is constant to ± 1 mA over the length of the pulse, during which time the source operates as stated above.

The duoplasmatron is capable of producing proton currents well in excess of 100 mA. The peak current in the experiment was limited by the acceptance of the emittance probe to 30 mA or less. A table of typical operating parameters follows:

Duoplasmatron parameters	
filament current	18-23 Amps
filament voltage	2-3 Volts
magnet current	1-2 Amps
arc voltage	100-300 Volts
arc current	4-20 Amps
beam energy	30-45 keV
gas pressure	10^{-5} torr

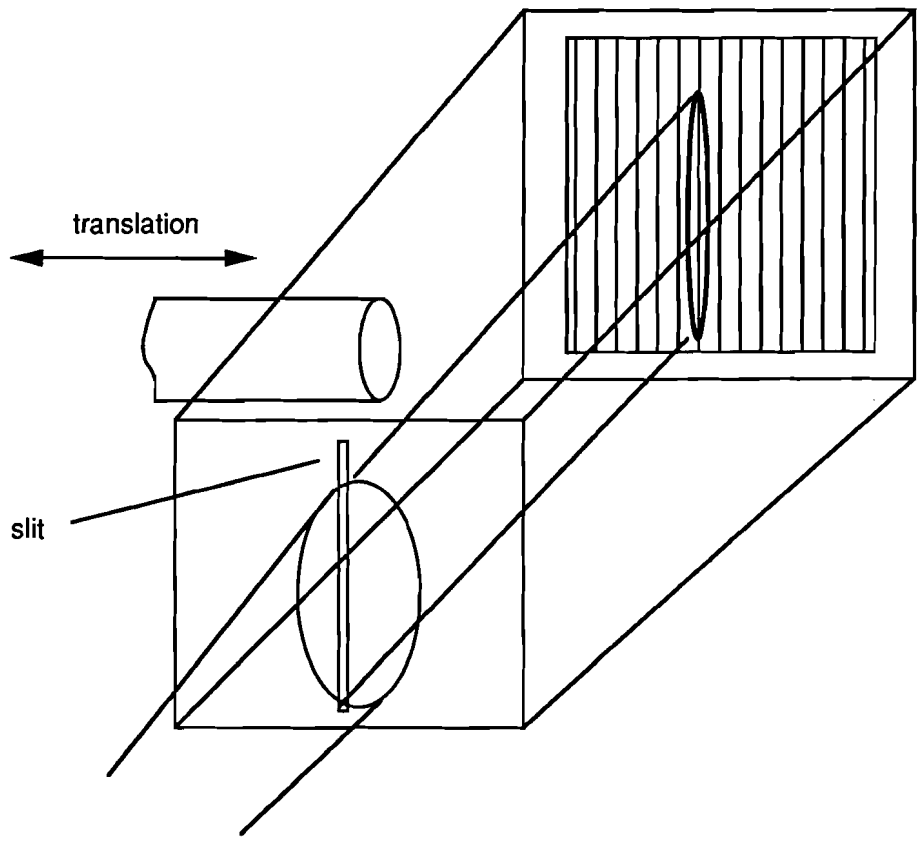

Figure 4.4: Emittance probe.

Beam Diagnostics

The primary diagnostic used in the experiment was the moving slit emittance probe. In addition to this there was a toroidal current transformer and a Faraday cup.

The moving slit emittance probe principle is illustrated in figure 4.4. The beam impinges on the front face of the probe, where a fraction of the beam passes through the slit, which is 51 μm in width. The probe face is assumed to be perpendicular to the beam axis. The "beamlet" thus selected then drifts for a

distance of 5 cm before hitting the backplane of the probe, which consists of 50 parallel wires (copper strips, actually), each with a width of 130 μm, separated by insulating kapton strips of $\sim$ 50μm width. Each wire strip is connected via a shielded cable to the input of one of the sample and hold modules discussed above.

By passing through the slit, the part of the beam within δx of x, where the slit has width $2\delta x$, has been selected. Within this beamlet there is some spread of angles $\delta x'$. Thus the beamlet will spread before it impinge on the wires.* The signals on the wires are proportional to the amount of current intercepted. The angle between the beam axis and a given wire is known since the wires and their insulating separators are of uniform width. Hence the distribution of wire voltages from the beamlet gives a discrete angular distribution for position x.

In practice the beam distribution is measured by "stepping" the emittance probe through the beam with a stepper motor, which can move in increments as small as 50 μm. The larger steps are multiples of 50 μm, i.e. the stepper motor steps are quantized. A typical step size was 200 μm. At each position, the wire voltages are read and digitized. When the run has ended, the data file is written to the Sun disk.

In order to help understand why the emittance probe measures the distribution of beam intensity $I(x, x')$, it helps to imagine a rectangular region of the x, x' plane centered at the origin. This region is divided up into smaller rectangles which measure δx by $\delta x'$. Each such rectangle then corresponds to a single

*The spreading of the beamlet due to space charge forces can be estimated analytically and is found to be < 1 % of the separation between adjacent wires for a 30 mA, 30 keV beam with a width of 1 cm, so it can be safely neglected.

wire reading at a particular x. The width δx corresponds to the step size, while the height $\delta x'$ is the separation between the wires. The wire voltage is a number stored in the smaller rectangle. Each step of the probe fills in a narrow strip of rectangles situated at x and ranging over $50\,\delta x'$ in the x' direction. When all the steps are done, the entire area is filled in and we have sampled $I(x, x')$ in the region.

The Faraday cup is essentially an open ended cylinder which intercepts the beam to provide a direct measurement of the beam current. A 100 Ω resistor was placed between the cup body and ground. The voltage on the cup was then viewed on the oscilloscope display. A fine wire grid biased to several hundred volts negative is placed approximately one cm in front of the cup to suppress secondary electron emission, which would give a false reading of the current otherwise.

The beam toroid is essentially a transformer with the beam as a single turn primary and the output signal taken from the secondary. The body of the toroid is a high magnetic permeability material with the secondary windings wrapped around it. In addition there is a resistance R_s in the secondary. With the proper choice of R_s and the number of turns in the secondary, the output voltage will follow the input voltage for signals of short duration. The beam pulse used was 90 μs in length.

4.2 Gabor Lens

As we stated above, the Gabor lens was studied because it has an azimuthally symmetric focusing field and it neutralizes the beam space charge. The question

that needs to be answered is whether or not the Gabor lens has sufficient optical quality to match a beam into an RFQ. Since the focus required at the input to the RFQ is very sharp, the lens used to focus the beam must be nearly free of aberrations. In particular the spherical aberration should be small. However, it is not possible to eliminate spherical aberration in an azimuthally symmetric lens such as a Gabor lens. [25]

4.2.1 Design of the Gabor Lens

The first Gabor lens was built in June, 1987. The coil for the solenoid magnet was designed with a power dissipation of ~ 750 watts and a central field of ~ 500 Gauss. The magnet was water cooled with hollow magnet wire. In addition multiple anodes were built inside of the lens in order to control the potential variation inside of the nonneutral plasma. This was found to be of little use. Observations of nonneutral plasmas show that when placed in an azimuthally symmetric external confining field provided by a single cylindrical electrode the plasma tends to reach a state in which the plasma interior is of uniform density with an edge region in which the density drops to zero in a distance on the order of one Debye length. [11] Uniformity of the interior density is what is needed for good focusing, so there is really no need to try and control the plasma potentials with multiple exterior anodes. It is more important to shape the profile of the magnetic field, since this has a greater effect on the density. Ideally one would have a uniform B field in the region occupied by the plasma.

4.2.2 Magnetic Field of the Lens

When it was built, the first lens did not work as well as was hoped. After some understanding of the physics of the nonneutral plasma was gained, we realized that the central field could be at the level of $\sim$ 200 Gauss to maintain the desired density of $10^{10} cm^{-3}$. This is a consequence of equation (3.4). Some of the literature on the Gabor lens contains incorrect results; namely, the nonneutral plasma physics is not handled correctly. This created confusion in the early going.

As mentioned above, we found that the unshielded field of the lens magnet disturbed the operation of the duoplasmatron. This is not surprising, since the duoplasmatron principle depends on the magnetic field being concentrated in the gap between the IE and the anode/expansion cup. With the Gabor lens magnet energized, there was a stray field in the region of the duoplasmatron of approximately 10 Gauss.

A second design (figure 1.1) was conceived with two separate magnet coils instead of one. The coils were constructed of solid core wire with no water cooling necessary. The main coil was constructed with 206 turns, the smaller "buck" coil with 80 turns. The power level of the main coil in the new lens was only 50 watts, an order of magnitude less than the previous magnet. Two coils were used in order that a cusp could be created in the magnetic field, i.e. a place where the field on the symmetry axis went to zero and then reversed. This was done in order to increase the stability of the plasma, as discussed above.

Computer calculations using the POISSON code were done to compute the magnetic field of the Gabor lens magnet. [31] POISSON uses a "successive point

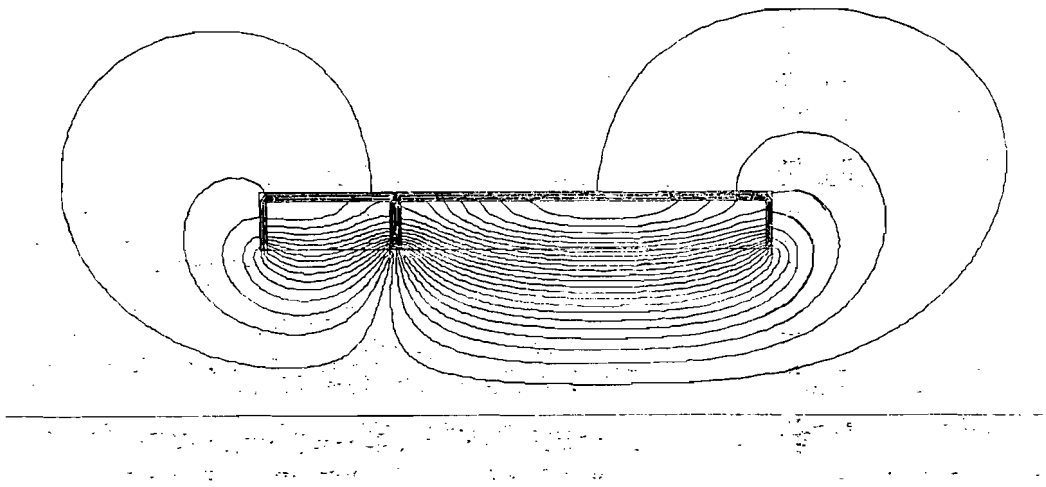

Figure 4.5: Magnetic Field of the Gabor lens.

over-relaxation" method to compute magnetostatic fields for the region of interest. The solution is done on a grid which is computed by a separate program AUTOMESH.

Because the magnetic field was interfering with the operation of the duoplasmatron, an iron shield was added to provide a return path for the flux. An estimate of the field in the region of the source found it to be comparable to the earth's field, i.e. less than 1 Gauss, with the shield in place. Experimentally, it was observed that the magnet did not affect ion source operation after installation of the new lens. A plot of the magnetic field lines is shown in figure 4.5.

4.3 Beam Measurements

4.3.1 Measurement of the Emittance

There were two sets of emittance measurements done. The first set involved passing the beam through the Gabor lens and measuring the emittance before the lens and afterwards in order to determine the effect of the lens. The second set of measurements was done solely on the "young" beam immediately out of the ion source. The emittance seen out of the source depends on many factors. An important part of the experiment was finding a way to measure the emittance in a reproducible fashion, which was accomplished by varying the extraction voltage of the Pierce geometry accelerating column. The extraction voltage is the potential difference between the anode and the first electrode of the column.

It was found that for any setting of the ion source parameters used to produce extracted beam, there was a minimum value of emittance that was obtained as the extraction voltage was varied. This is shown in figure (4.6). The procedure to acquire data that was used for the second set of measurements was to change the ion source arc voltage and the accelerating voltage to produce a desired energy and current, then the extraction voltage was varied until a minimum emittance was found. This ensured that the beam was matched into the accelerating column.

By varying the extraction voltage, the shape of the "plasma emissive meniscus" from which the beam is extracted in the expansion cup of the duoplasmatron is changed. [28] This directly affects the angular distribution of the emitted beam, since ions tend to leave along trajectories normal to the meniscus. Since the shape of the distribution function $f(x, x')$ is changed, the emittance changes.

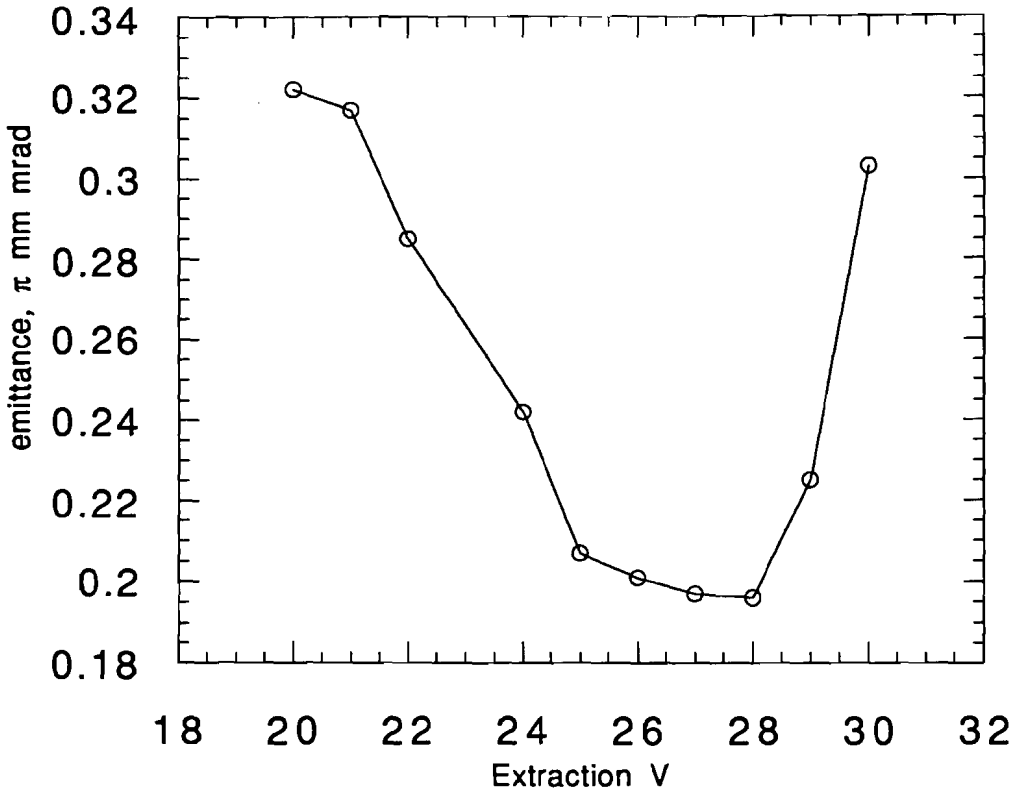

Figure 4.6: Emittance vs. extraction voltage.

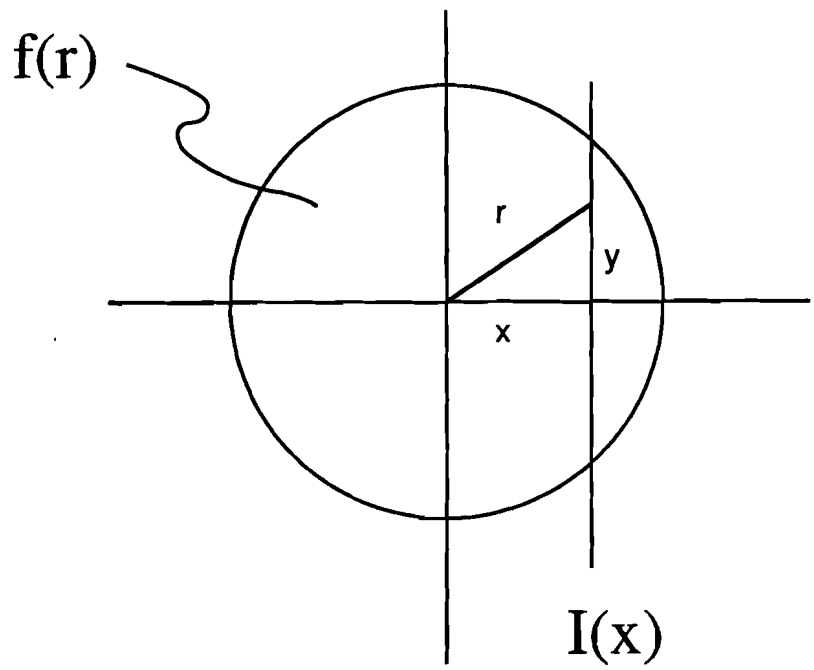

Figure 4.7: Geometry for Abel transform.

4.3.2 Abel Inversion of the Density Profile

As we mentioned above, the emittance growth of a space charge dominated beam is driven by the electrostatic field energy of the beam. Thus we are interested in calculating the electrostatic field energy from the measured distribution function of the beam. A necessary part of this process is the Abel inversion of the density profile. It is easy to extract the distribution $f(x)$ from the measured data. Since the beam is azimuthally symmetric, what is needed to calculate the electric field is $f(r)$. With $f(r)$ in hand, it is straightforward to calculate the electric field by solving Poisson's equation.

Consider the measurement of the beam distribution by a moving slit emittance probe (figure 4.7). The intensity of the integrated signal measured at a particular

value of x, $I(x)$, is given by

$$I(x) = \int_{-\infty}^{+\infty} f(r)dy. \tag{4.1}$$

Using the fact that x, y, and r are related by the Pythagorean theorem as shown in the figure, dy can be expressed in terms of dr to yield

$$I(x) = 2\int_{x}^{+\infty} \frac{rf(r)dr}{\sqrt{r^2 - x^2}}. \tag{4.2}$$

We say that $I(x)$ is the Abel transform of $f(r)$. This is an integral equation which must now be solved for $f(r)$, the quantity of physical interest. The solution can be written as [4]

$$f(r) = -\frac{1}{\pi}\int_{r}^{\infty} \frac{\left(\frac{dI}{dx}\right) dx}{\sqrt{x^2 - r^2}}. \tag{4.3}$$

The literature on the numerical evaluation of (4.3) is large. This is not a form which is suitable for application to experimental data, for several reasons. There is a singularity in the integrand, and the evaluation of the derivative dI/dx tends to introduce large errors, since the intensity $I(x)$ is discretely sampled. We would therefore like to express the inverse transform in a different form. Also, real data has a noise component, which can be amplified by the inversion process, particularly for points near the origin. [40] It is desirable to remove the noise as much as possible while processing the data. Fortunately, this can been done. It can be shown that the Fourier, Hankel, and Abel transforms form a set known as the FHA cycle; i.e., applying the Abel transform and then the Fourier transform to a function, we obtain the Hankel transform.[4] The Fourier and Hankel transform can be computed with fast Fourier transform (FFT) algorithms, thus decreasing the computation time required. [39]

We can write the Fourier transform of (4.1) as

$$\mathcal{F}\{I(x)\} = \int_{-\infty}^{+\infty}\int_{-\infty}^{+\infty} f(r)exp(-i2\pi xq)dxdy \tag{4.4}$$

Using an identity from the theory of Bessel functions, [3] we can rewrite (4.4) as

$$\mathcal{F}\{I(x)\} = 2\pi\int_{0}^{+\infty} rf(r)J_0(2\pi rq)dr \tag{4.5}$$

We recognize the right hand side of (4.5) as the Hankel transform of $f(r)$. The inverse Hankel transform is identical to the forward Hankel transform, hence if we take the inverse Hankel transform of (4.5), it can be written

$$f(r) = 2\pi\int_{0}^{+\infty} qJ_0(2\pi rq)\int_{-\infty}^{+\infty} I(x)exp(-i2\pi xq)dxdq \tag{4.6}$$

This is the form which was used for the inversion of the experimental data. This equation has several advantages over (4.3). There is no singularity in the integrand. The data can be filtered in the transform domain to smooth it after application of the FFT. [20] Considering the baseband nature of the data, a low pass filter is appropriate. A filter with a bandwidth of 0.2 times the Nyquist frequency was used. This smoothing is an important part of the Abel inversion process. Without smoothing the output would contain noise which is the Abel transform of the input noise. The use of FFT routines increases the speed with which the calculations can be done on a computer, and the absence of the derivative removes a source of (numerical) uncertainty in the analysis.

Source code for a program to perform the inversion was obtained, modified to suit our data, and debugged. [39] The FFT is implemented using a standard algorithm. [5] The Hankel transform is calculated with a method due to Candel which uses the FFT. [7] The routine was tested in several ways. One test is to

input a Gaussian. It is easy to show using the defining equation (4.1) that the Abel transform of a Gaussian distribution is a Gaussian. A test input

$$I(x) = exp(-x^2/400) \tag{4.7}$$

was used. The inverse transform of (4.7) can be easily calculated from (4.3). The result is

$$f(r) = \frac{1}{20\pi} exp(-r^2/400) \tag{4.8}$$

which is easy to show. Thus the output of the inversion routine can be checked against a known inverse in this instance. If the filtering is good, then the computed inverse will agree well with the calculated inverse. Equation (4.7) was finitely sampled at 256 evenly spaced points on the interval $[-100, 100]$ and input into the inversion routine. In addition, a random sequence with uniform deviation on the interval $[-0.05, 0.05]$ was added to I. The result of the inversion calculation is shown in figure (4.8). Other test inputs were applied for which the inverse could be calculated analytically to compare with the output of the computer program. A "waterbag" distribution was input as a second test. The form of the waterbag distribution in the x coordinate is

$$I(x) = \begin{cases} C(a^2 - x^2)^{3/2} & |x| \leq a \\ 0 & \text{otherwise} \end{cases} \tag{4.9}$$

where a is a constant that defines the edge of the beam and C is the normalization constant. The result of this inversion is shown in figure (4.9). As before, we compare the result with the analytically calculated inverse function,

$$f(r) = \begin{cases} \frac{3}{4}C\left(1 - \frac{r^2}{a^2}\right) & r \leq a \\ 0 & \text{otherwise,} \end{cases} \tag{4.10}$$

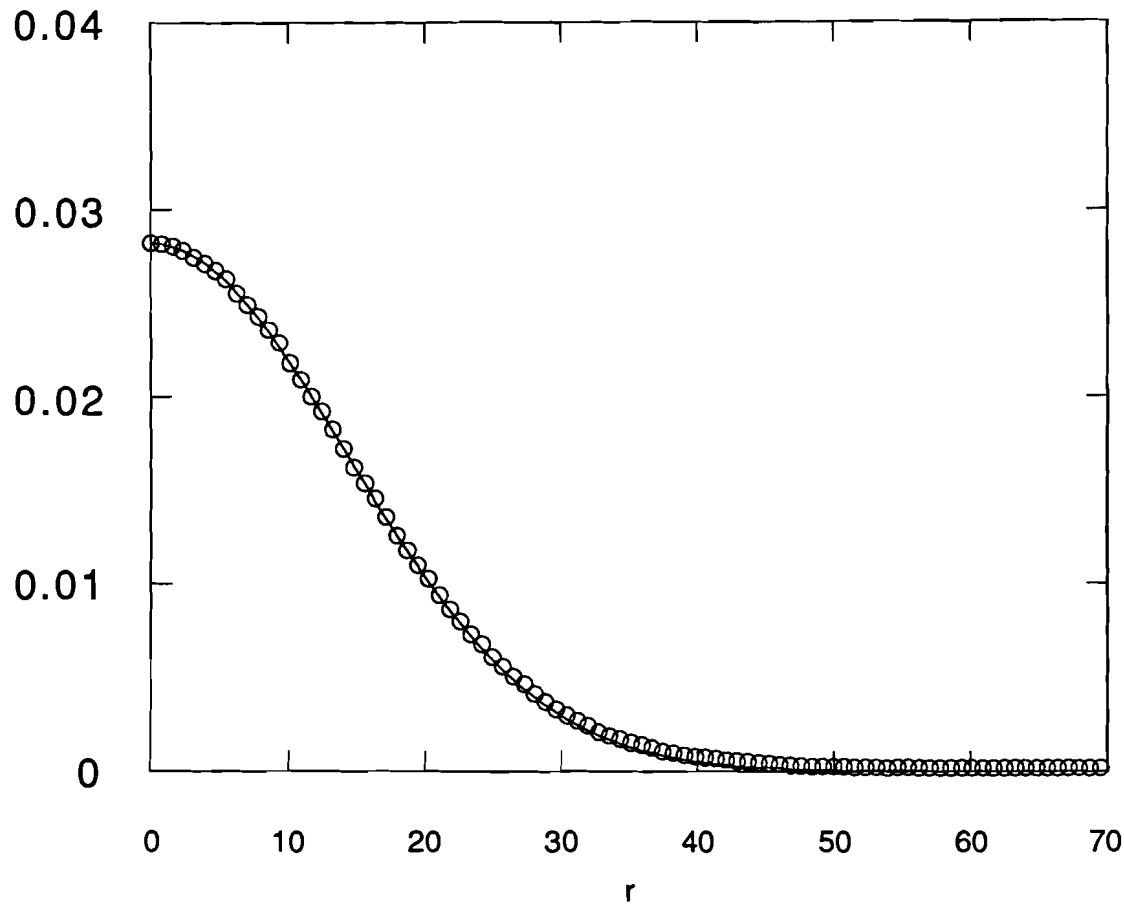

Figure 4.8: Abel inverse of Gaussian input distribution. The circles represent the output of the computer program; the solid line is the calculated inverse. The normalization of f is arbitrary.

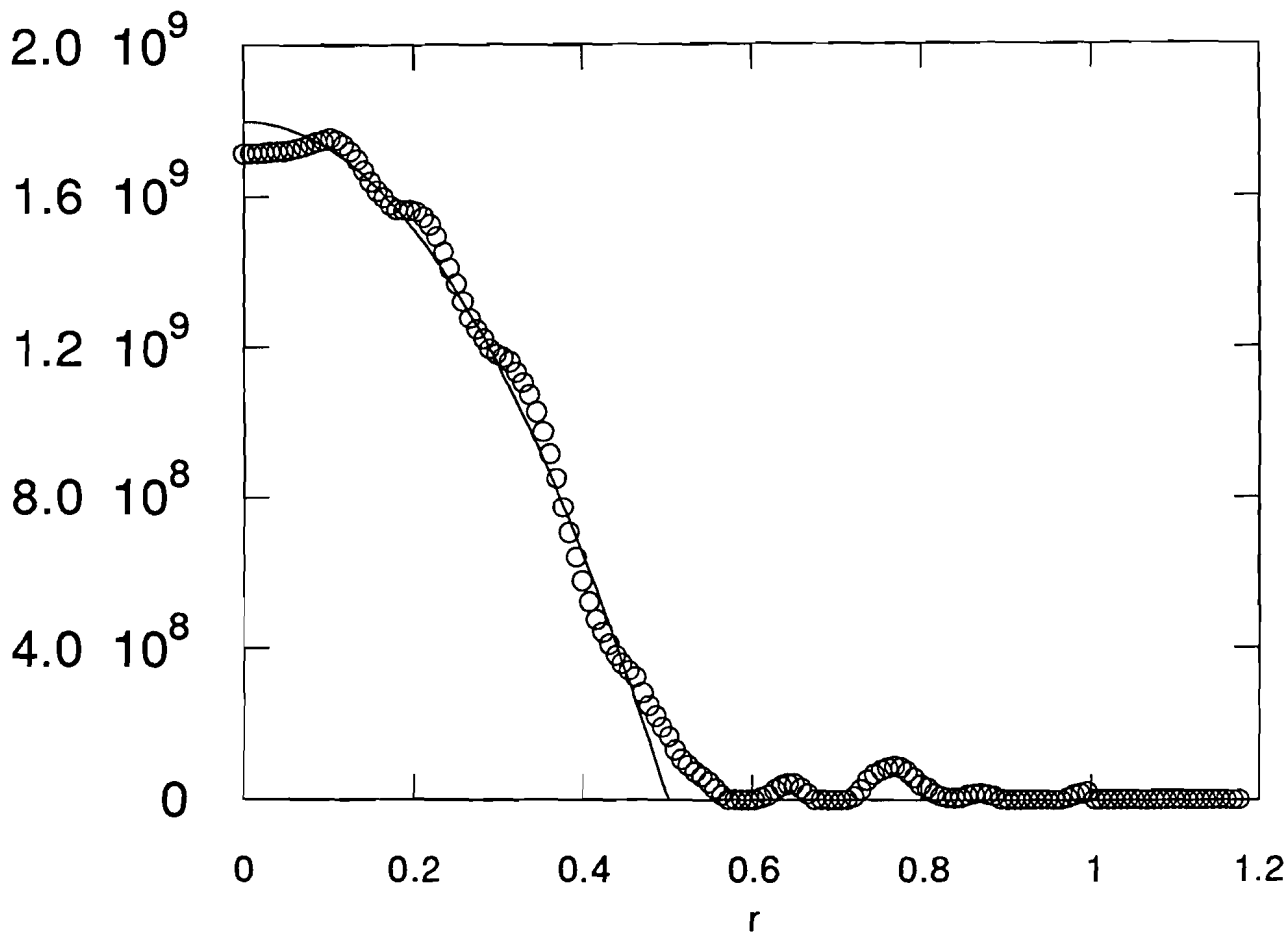

Figure 4.9: Abel inverse of waterbag input distribution. The circles represent the computer calculated inverse, the solid curve is the analytic inverse.

where C and a are the same as above. The results of these two test cases indicate that the inversion routine is effectively filtering the input noise and calculating the correct inverse for these functions. It is possible to find slightly more pathological input functions for which the output shows spurious oscillations. In particular, these oscillations are seen for an input in which the function falls sharply to zero, e.g. a Heaviside step function in x. This is a manifestation of the Gibbs phenomenon.[3] In all such cases which were studied, the addition of noise actually improves the results, since noise tends to blur any "hard" edges the function might have.

4.3.3 Calculation of the Electrostatic Field Energy

Given the radial distribution function $f(r)$, it is straightforward to calculate the electrostatic field energy of the beam. To be more precise, we calculate the field energy per unit length of the beam W, since that is the quantity which enters into the theory. For an azimuthally symmetric beam, that quantity is given by (1.20). This calculation was done by a subroutine **ecalc**, which was called from the main inversion routine. Simpson's rule was used to do the integration. Since the inverted distribution contained random errors at the level of a few percent relative to the signal strength, it was not necessary to use a more sophisticated routine. Simpson's rule was adequate for these calculations.

Ecalc worked in two steps. The input to the subroutine was the distribution $f(r)$ obtained from the inversion procedure. Before the electric field is calculated, the distribution is normalized. It follows from continuity considerations that the

correct normalization constant N is

$$N = \frac{I}{2\pi q v \int_0^R r f(r) dr} \tag{4.11}$$

where I is the beam current, q is the magnitude of the proton charge, and v is the speed of the beam particles $\sqrt{2T/m}$. The first integration obtained the radial electric field:

$$E_r = \frac{1}{\varepsilon_0 r} \int_0^r r' \rho(r') dr'. \tag{4.12}$$

With the electric field in hand, the field energy per unit length can be calculated using (1.20). The result of this series of calculations for a real beam is shown in figure (4.10). It is noticeable that the function $W(r)$, the electrostatic field energy per unit length as a function of r, is a very smooth function of r. This is not surprising, since it was obtained after two integrations of $f(r)$, a function with some slight undulation. The high frequency noise evident in $I(x)$ is completely gone after Abel inversion to obtain $f(r)$. It has to be remembered that the uncertainty in $f(r)$ is largest near the origin of r when comparing the results of two inversions. Since it is the product $rf(r)$ which is integrated to obtain $E_r(r)$, this does introduce uncertainty into W. This was born out in the experiments, which showed that W varied by $\pm 5\%$ over a set of 10-20 runs taken with identical ion source parameter settings.

4.3.4 Data Interpretation

The two most important quantities observed were the beam emittance and the electrostatic field energy of the beam distribution. We recall that it is the electrostatic field energy that drives the emittance growth. There were a total of 366

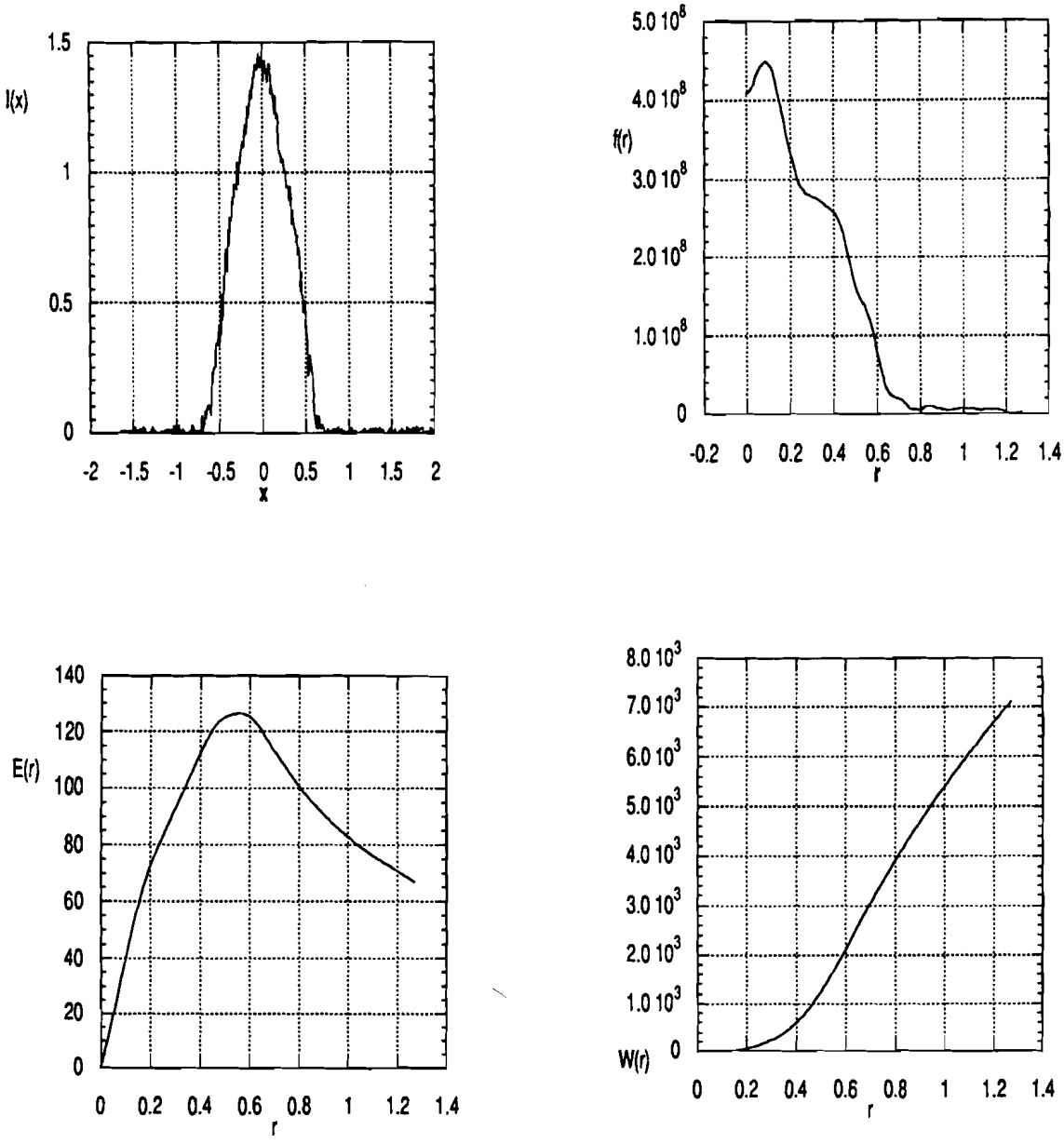

Figure 4.10: Input x density, Inverted density $f(r)$, electric field, and electrostatic field energy $W(r)$ for 45 keV proton beam.

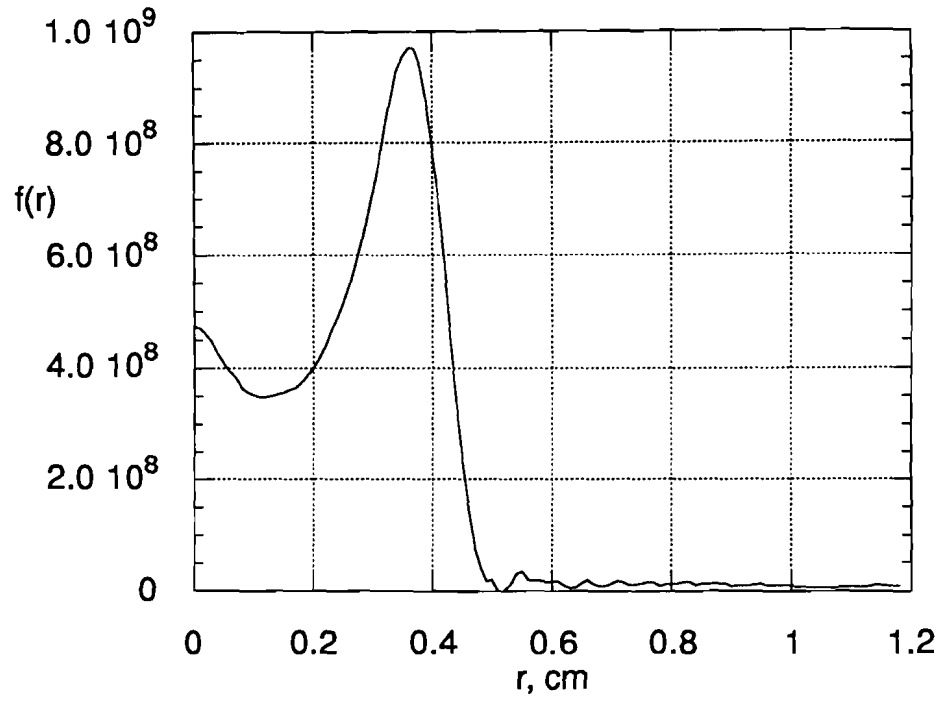

Figure 4.11: "Hollow" beam distribution. The units of f are cm^{-3}.

emittance runs studied.

The Shape of the Function $f(r)$

One observation that was made concerns the shape of the function $f(r)$. Emittance was measured at three different positions along the beam axis. We shall call them z_1, z_2, and z_3. At position z_1, we observed that the beam had a hollow shape. This is illustrated by the distribution in figure (4.11), which shows the result of the Abel inversion procedure for a single emittance run. This shape can be changed some by varying the ion source parameters. However, we found that the hollow shape was predominant at the z_1 position with the extraction optics

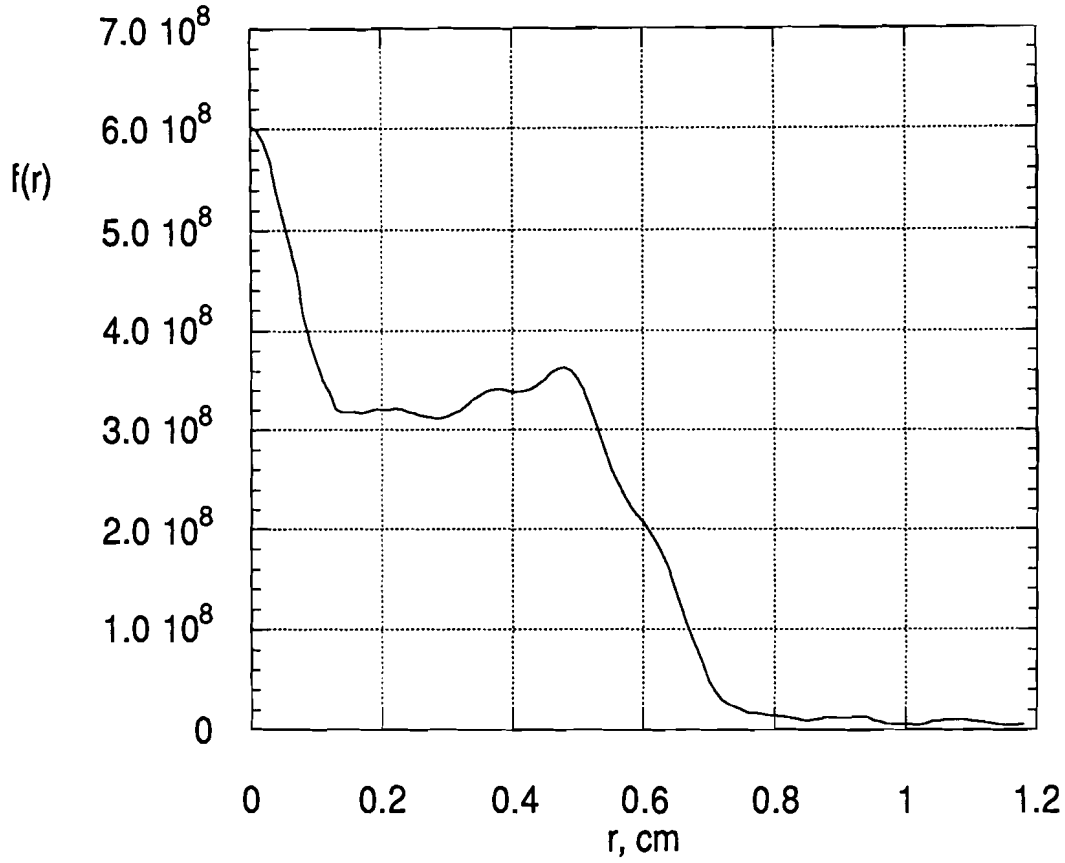

Figure 4.12: Sample beam distribution at the z_2 position.

tuned for minimum emittance as stated above.

When we moved the emittance probe out 5.9 cm to z_2, we found that the beam was no longer hollow. It had assumed more of a flattened shape, with a "peak" in the middle. See figure (4.12). As before, the figure corresponds to a single emittance run. Moving another 2.5 cm to position z_3, the beam has assumed an even more pronounced peaked shape in its distribution. This is shown in figure (4.13), which is for a single run. The interpretation is that the particles on the edge of the beam at position z_1 have moved into the region near the beam axis

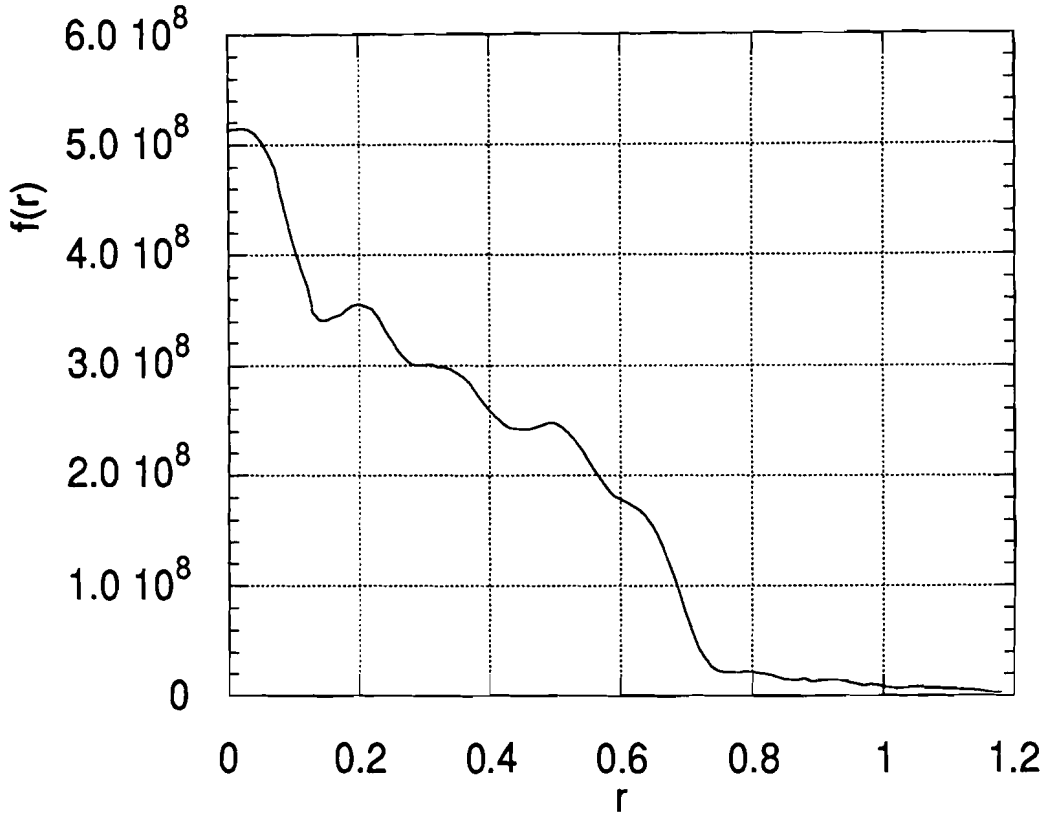

Figure 4.13: Sample beam distribution at the z_3 position.

due to an inward component of radial velocity. Of course, the space charge of the beam also contributes to development of this shape, although it is not easy to untangle the two contributions.

Field Energy

An important part of the theory of space charge dominated beams is the statement of energy conservation given by

$$T + W = const. \tag{4.13}$$

where W is the field energy of the beam, defined above, and T is given by

$$T = p_z \left\langle x'^2 \right\rangle \left(\frac{I}{q}\right), \tag{4.14}$$

where $x' = p_x/p_z$. This equation is derived from a similar result in the literature. [18] Physically, T is the transverse kinetic energy per unit length of the beam. As part of the data analysis, the two quantities T and W were tabulated for each emittance run. Examination of histograms of these quantities for each of the three positions z_1, z_2, and z_3 shows that $T + W$ is constant within the statistical spread in the data. This is in agreement with the theory. The results, tabulated from all of the data, are shown in the following table.

$T + W$	position, cm
$(2.9 \pm 1.6) \times 10^{-6}$	0.0
$(5.1 \pm 3.2) \times 10^{-6}$	5.9
$(6.5 \pm 3.5) \times 10^{-6}$	8.4

Since (1.4) predicts that the emittance growth depends on the field energy of the beam, one might expect to see a correlation between field energy W and emittance. No clear correlation is seen in the data, plotted in figure (4.14). This plot shows data from 338 emittance runs.

There is a correlation found between W and the perveance K, which is proportional to $I/V^{3/2}$. This relationship is plotted in figure (4.15). This data set is fit rather well with the simple inverse relationship shown in the figure. It is unknown exactly why this dependence seems to apply.

There is another correlation found between the quantity U of equation (1.4) and the rms width of the beam. This is plotted in figure (4.16). This particular

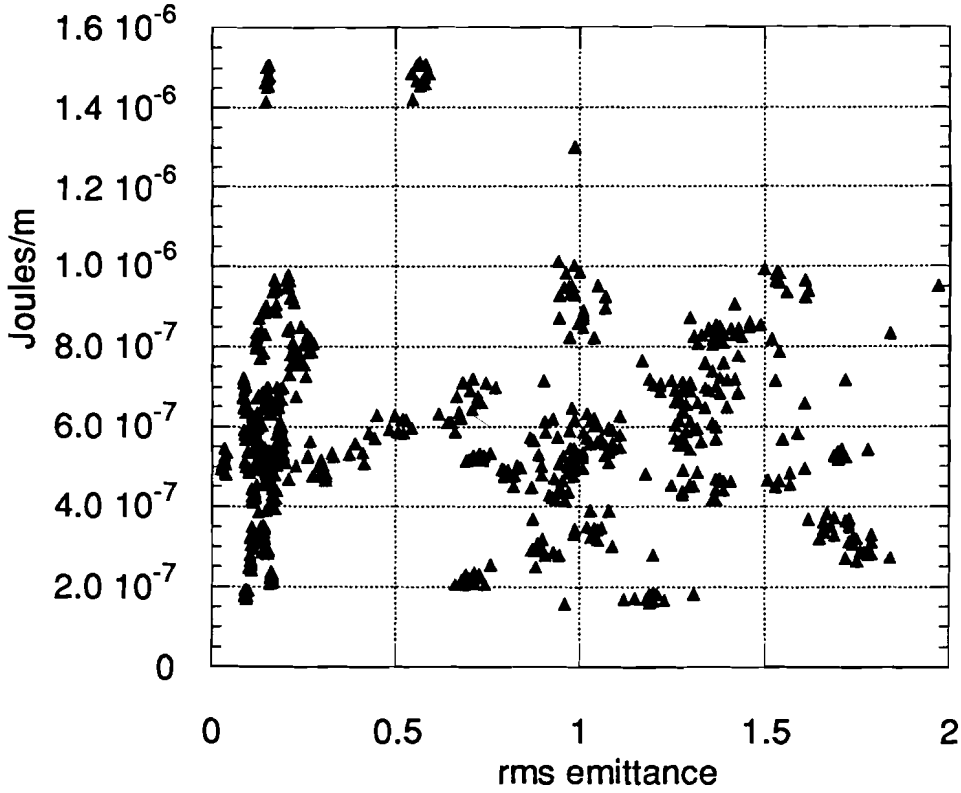

Figure 4.14: Field energy W vs. RMS emittance.

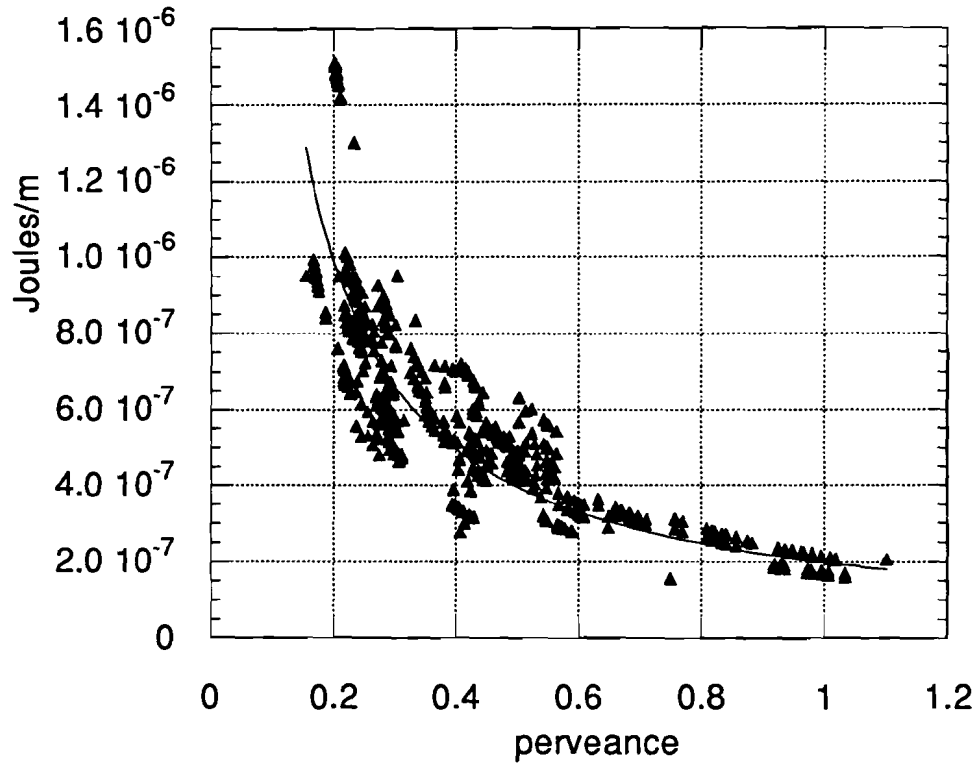

Figure 4.15: Field energy W vs. perveance. The data is fit to the curve $(1.98 \times 10^{-7})/x$.

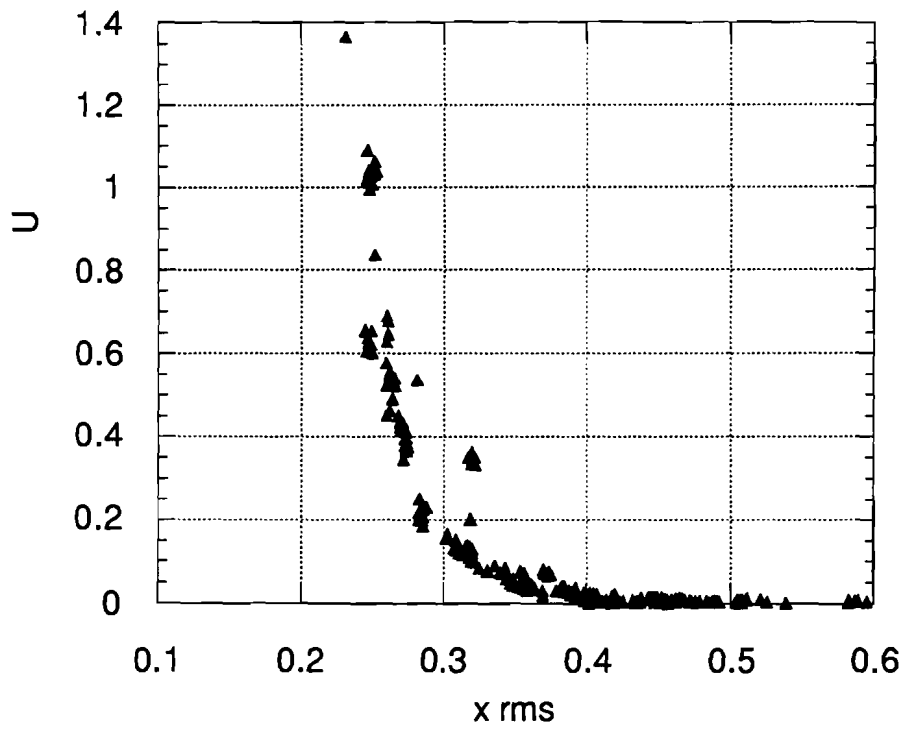

Figure 4.16: Nonlinear field energy U (dimensionless) vs. rms beam size in cm.

correlation was unexpected when first seen in the data. This is perhaps the most striking relationship found in the data. There is as yet no satisfactory quantitative explanation for it. Qualitatively, the relationship is that the smaller beams have more nonlinear field energy. This quantity is strongly dependent on the shape of the distribution function. It must be considered to be a property of the duoplasmatron. Although it is not shown on the graph, the points with the largest U values come mostly from the emittance measurements at position z_1, immediately outside the exit of the ion source.

Emittance Growth

Perhaps the most dramatic prediction of emittance growth theory is the large "explosive" growth of emittance that a beam experiences when injected into a uniform focusing channel. Recall that this growth is predicted to occur in a distance $\lambda_p/4 = m\omega_p/p_z$. A number of comments are appropriate before we reach a conclusion on the nature of any such growth in the data presented here.

The rms emittance is calculated from formula (2.12). Rms fitting procedures suffer from a sensitivity to outliers; that is, a small subset of data points that are far from the mean can contribute a large amount to the rms value. In our case, these outliers came from electrical noise on the wires in the emittance measuring apparatus. Thus it is important to understand something about the nature of this noise. A histogram plot of the noise signal on the emittance wires is shown in figure (4.17). These readings were taken by simply digitizing the wire voltages in the emittance probe with the probe positioned out of the beam. We see that there are no counts with a voltage greater than 0.0134 volts. This is to be contrasted

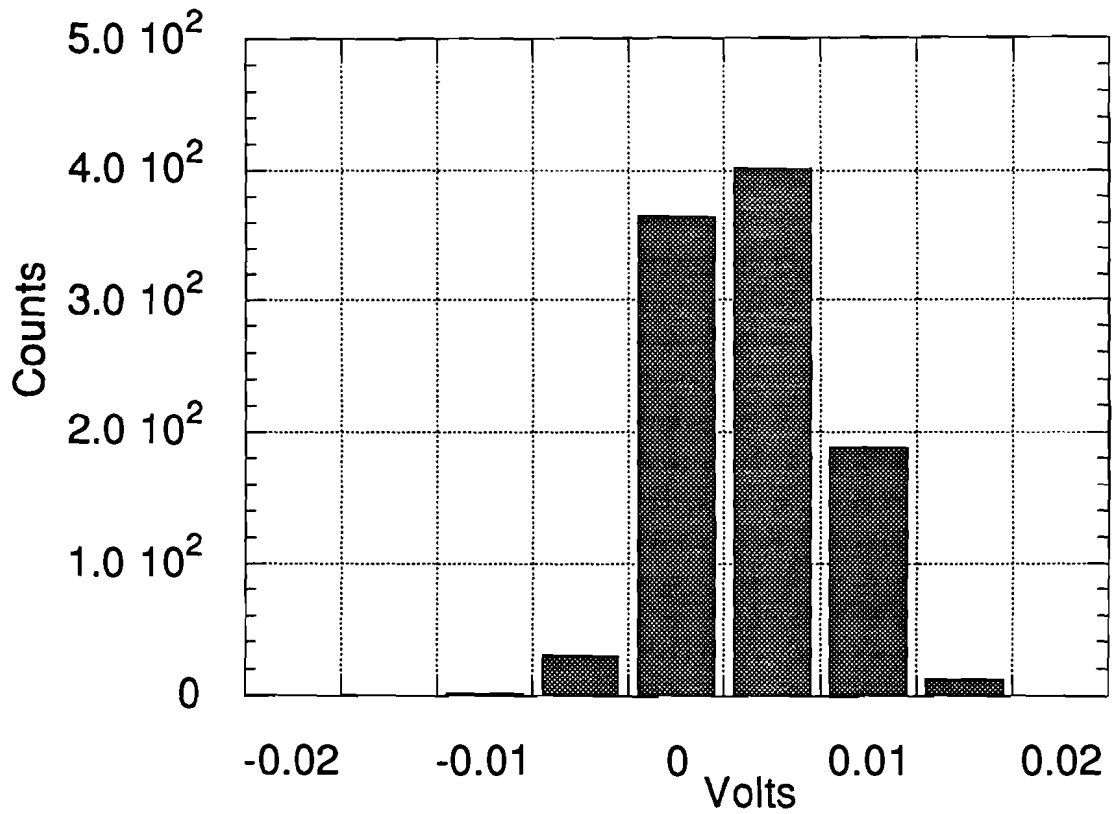

Figure 4.17: Noise readings on emittance wires.

with a plot of the wire voltages from the same voltage range of an actual run; see figure (4.18). In both cases the distribution had a mean value near zero. For the noise signal we find statistically

$$V = (3.9 \pm 3.9) \times 10^{-3} Volts \tag{4.15}$$

while for the same range of a actual run,

$$V = (0.0 \pm 1.0) \times 10^{-2} Volts. \tag{4.16}$$

Statistically, then, there is no significant difference between the voltages in the range < 0.0134 volts when the probe is in the beam and when it is out of the beam. We note that for the run plotted in figure (4.18), there were 11,000 wire readings stored, 9,870 of them being within the range of the noise levels.

The effect of the noise on the rms emittance calculated from the data was to cause the output rms emittance to be much larger than the true rms emittance of the beam. The outliers introduced by noise could increase the rms emittance by a factor of 2-4. In order to eliminate this spurious contribution to the emittance, a cut was taken at the 0.015 volt level. Unless stated otherwise, this cut was used for all the data presented here. This was implemented by setting all wire voltages to zero if the stored value was less than the cut level. We see from the numbers presented above that approximately 10 % of the wire readings in a typical emittance run contribute to the calculation, the other 90 % being noise which is discarded.

As was done with the field energy data, it is possible to tabulate the average rms emittances for the three positions at which emittance data was taken. This is

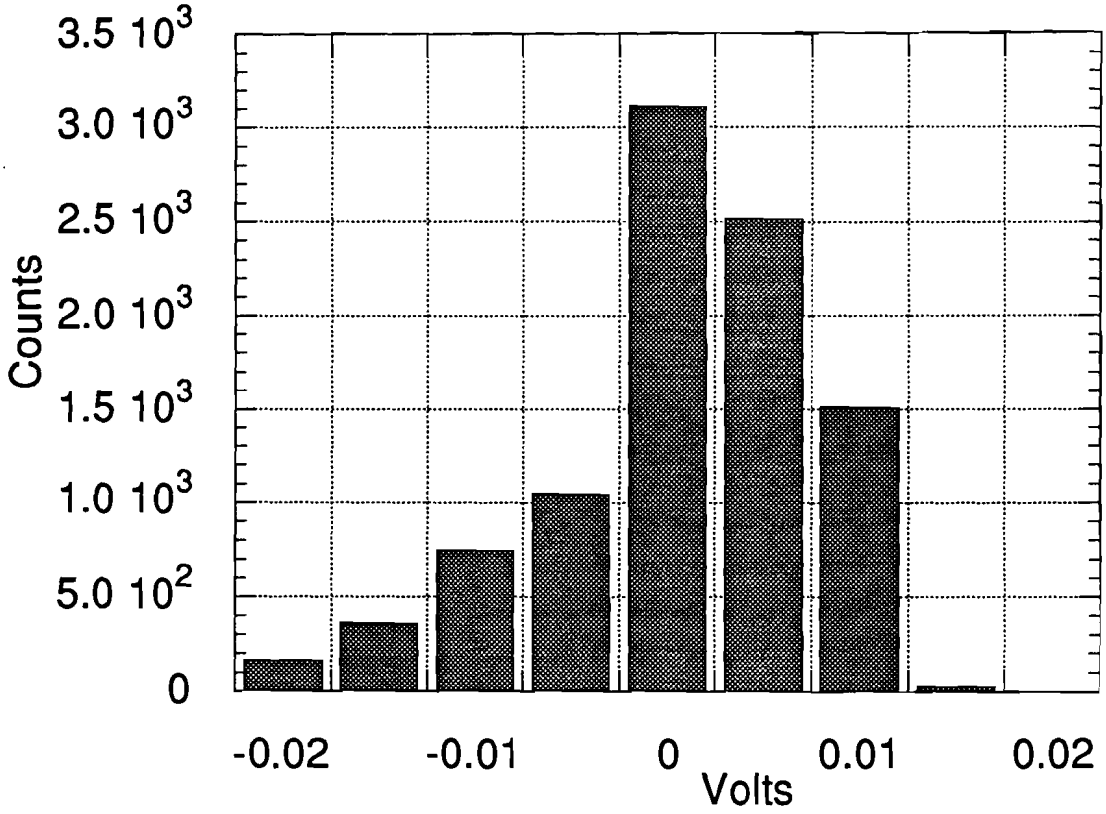

Figure 4.18: Low level readings on emittance wires from an emittance run.

shown in the following table. The units of emittance are conventionally expressed as "$\pi\ mm \cdot mrad$."

$RMS Emittance$	position, cm
$0.98 \pm .31$	0.0
$1.02 \pm .32$	5.9
$1.6 \pm .15$	8.4

This is because of the well known formula relating beam width, the beta function β, and emittance: [12]

$$x = \sqrt{\frac{\varepsilon\beta}{\pi}} \tag{4.17}$$

Having the π in the units is convenient for calculation.

There is no statistically significant growth in the rms emittance as the beam propagates from z_1 to z_2, a distance of 5.9 cm. As the beam moves from z_2 to z_3, however, the emittance has grown by a factor of 1.6. The typical value of $\lambda_p/4$ for the beams measured was 13.3 cm. This certainly qualifies as an explosive growth. Simulations published in the literature often neglect the emittance of the initial beam, and also assume that the beam is subjected to an external force field. In addition, the initial distributions are idealized abstractions which do not completely simulate the charge distribution of a real beam. It is not clear how to relate this observation of emittance growth in a drifting beam to published emittance growth curves. It is plausible that the sharp growth seen is sharply dependent on the initial distribution.

We have found that almost all of the emittance growth is due to particles in the "halo" of the beam, i.e. particles which are positioned near the edge of the distribution in phase space. Figure (4.19) is an illustration of this effect. This

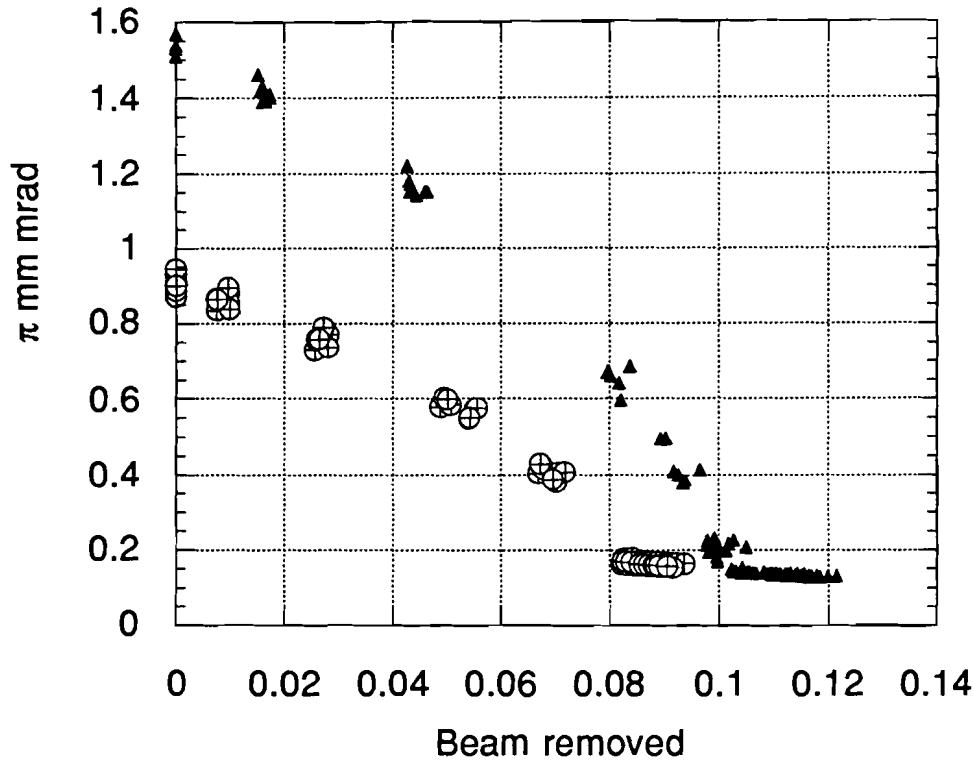

Figure 4.19: RMS emittance vs. fraction of beam removed.

figure was produced by taking two sets of emittance runs and then increasing the level of the cut from the minimum level (0.015 volts) upward until there was no emittance growth evident at all. Then the fraction of beam removed is calculated. This is proportional to the volume of the distribution that is removed, i.e. the change in the integral

$$V = \int \int f(x, x')dxdx'. \tag{4.18}$$

We see that all of the emittance growth is due to the approximately 10 % of the beam particles which are in the halo of the beam. In the core of the beam, the curve is flat. In the upper curve, which represents data from position z_3, a larger percentage of the beam has moved into the halo. This contributes significantly to the rms emittance.

Chapter 5

CONCLUSION

We conclude this work with a summary of what we have done and a few statements about future work on low energy space charge dominated beams.

This thesis was largely experimental in nature. There has been much excellent theoretical work published in the field of low energy beam transport. We have done some new measurements to test the most important part of that theory, the theory of emittance growth. In the course of the experiments, we found that accurately testing the emittance growth theory was quite difficult to do. This is often the nature of experimental work. The results obtained are not inconsistent with the theory. This is not surprising, since it is well founded in classical physics. We have found some new correlations which were not predicted by the theory.

It is a well known fact that emittance grows for almost any beam as it propagates through almost any kind of transport line or accelerating structure. We undertook to study the particularly rapid growth of emittance which occurs in a space charge dominated beam over a relatively short distance. The dynamics

of this process for a cold space charge dominated beam were predicted to show an explosive growth, and that has been observed. Another important prediction is the constancy of the field energy sum for a drifting beam, $T + W$. This also is verified, although not with high precision. We have found that the emittance growth observed is due entirely to particles in the halo of the beam. If a cut is taken in an emittance run data set which removes 10 % of the beam particles, the emittance growth vanishes.

In conclusion, then, it is hoped that others will continue to experiment with low energy space charge dominated beams, in the hopes of improving existing accelerator facilities and discovering new ways to transport low energy beams. Other technologies which would benefit include heavy-ion fusion, which may provide a source of cheap power in the years to come. Accelerators are also finding use as cancer treatment tools, and the improvement of their low energy injector systems can only help this field. There is much work to be done, and we have only explored a small nook of the available parameter space.

Bibliography

[1] C. Agritellis, R. Chasman, and Th.J.M. Sluyters. Design of the low-energy beam transport system of the brookhaven 200-mev injector linac. *Transactions in Nuclear Science*, 1969.

[2] O.A. Anderson. Internal dynamics and emittance growth in space-charge-dominated beams. *Particle Accelerators*, 21:197–226, 1987.

[3] G. Arfken. *Mathematical Methods for Physicists*, page 491. Academic Press, 1970.

[4] R.N. Bracewell. *The Fourier Transform and Its Applications.* McGraw-Hill, New York, 1977.

[5] E.O. Brigham. *The Fast Fourier Transform.* Prentice-Hall, 1974.

[6] L. Brillouin. A theorem of Larmor and its importance for electrons in magnetic fields. *Physical Review*, 67, 1945.

[7] S.M. Candel. An algorithm for the fourier-bessel transform. *Computer Physics Communications*, 23:343–353, 1981.

[8] F. Chen. *Introduction to Plasma Physics and Controlled Fusion.* Plenum Press, 1984.

[9] E.D. Courant and H.S. Snyder. Theory of the alternating gradient synchroton. *Annals of Physics*, 3:1–48, 1958.

[10] R.C. Davidson. Electrostatic shielding of a test charge in a nonneutral plasma. *J. Plasma Physics*, 6:229, 1971.

[11] R.C. Davidson. *Theory of Nonneutral Plasmas.* Advanced book Classics. Addison-Wesley, 1989.

[12] D.A. Edwards and M.J. Syphers. An introduction to the physics of particle accelerators. In M. Month and M. Dienes, editors, *Physics of Particle Accelerators.* American Institute of Physics, 1989.

[13] A.T. Forrester. *Large Ion Beams.* Wiley-Interscience, 1988.

[14] A. Frank, R. Mahler, and M.F. Shea. The dzero rack monitor module. D0 Note 1051, Fermi National Accelerator Laboratory, 1990.

[15] D. Gabor. A space-charge lens for the focusing of ion beams. *Nature*, 160, 1947.

[16] H. Goldstein. *Classical Mechanics.* Addison-Wesley, Reading, Massachusetts, 1980.

[17] P.W. Hawkes. *Lens Aberrations*, volume 1, chapter 25, page 422. Academic Press, 1967.

[18] I. Hoffman and J. Struckmeier. Generalized three-dimensional equations for the emittance and field energy of high-current beams in periodic focusing systems. *Particle Accelerators*, 21(2):69–98, 1987.

[19] J.D. Jackson. *Classical Electrodynamics.* John Wiley & Sons, New York, second edition, 1975.

[20] J.F. Kaiser and W.A. Reed. Data smoothing using low-pass digital filters. *Review of Scientific Instruments*, 48(11):1447–1457, 1977.

[21] I.M Kapchiskii and V.V. Vladimirskii. Limitations of proton beam current in a strong focusing linear accelerator associated with the beam space charge. In *Proceedings of the International Conference on High Energy Accelerators*, page 274 ff., CERN, Geneva, 1959.

[22] N.A. Krall and A.W. Trivelpiece. *Principles of Plasma Physics.* San Francisco Press, San Francisco, CA, 1986.

[23] L.D. Landau and E.M. Lifshitz. *Statistical Physics*, volume 1. Pergamon Press, third edition, 1982.

[24] P.M. Lapostolle. Possible emittance increase through filamentation due to space charge in continuous beams. *Transactions in Nuclear Science*, page 1101, 1970.

[25] J.D. Lawson. *The Physics of Charged Particle Beams.* Oxford University Press, New York, second edition, 1988.

[26] J.D. Lawson, P.M. Lapostolle, and R.L. Gluckstern. Emittance, entropy, and information. *Particle Accelerators*, 5(61), 1973.

[27] H.W. Lefevre, R.C. Connolly, D.P Xi, G.E. Sieger, and J.C. Overley. Can an electron plasma lens produce sub-micrometer size focal spots of mev ions? *Nuclear Instruments and Methods*, pages 707–712, 1985.

[28] C. Lejeuene. *Extraction of High-Intensity Beams from Plasma Sources: Theoretical and Experimental Treatments*, volume 13 C of *Advances in Electronics and Electron Physics*, pages 207–293. Academic Press, 1980.

[29] C. Lejeuene and J. Aubert. *Emittance and Brightness: Definitions and Measurements*, volume 13 A of *Advances in Electronics and Electron Physics*, pages 159–259. Academic Press, 1980.

[30] Allan J. Lichtenberg. *Phase-Space Dynamics of Particles.* John Wiley & Sons, Inc., 1969.

[31] M.T. Menzel and H.K. Stokes. User's guide for the poisson/superfish group of codes. Technical report, Los Alamos National Laboratory, 1987.

[32] S. Ohnuma. The beam emittance. EXP 111, Fermi National Acclerator Laboratory, 1983.

[33] J.A. Palkovic, F.E. Mills, C. Schmidt, and D.E. Young. Gabor lens focusing of a proton beam. In F. Bennett and J. Kopta, editors, *Proceedings of the 1989 IEEE Particle Accelerator Conference*, page 304, New York, 1989. IEEE.

[34] S.A. Prasad and T.M. O'Neill. Finite length thermal equilibria of a pure electron plasma column. *Physics of Fluids*, 22(2):278 – 281, February 1979.

[35] M. Reiser. Periodic focusing of intense beams. *Particle Accelerators*, 8:167–182, 1978.

[36] M. Reiser. Comparison of gabor lens, gas focusing, and electrostatic quadrupole focusing for low-energy ion beams. In *Proceedings of the 1989 IEEE Particle Accelerator Conference*, page 1744, New York, 1989. IEEE.

[37] F.J. Sacherer. Rms envelope equations with space charge. *Transactions in Nuclear Science*, page 1105, 1970.

[38] M.F. Shea. The fermilab 200 mev linac control system hardware. Technical Memorandum TM-1238, Fermi National Accelerator Laboratory, January 1984.

[39] L.M. Smith. Abel inversion using transform techniques. *Journal Quantum Spectroscopy and Radiation Transfer*, 39(5):367–373, 1988.

[40] L.M. Smith. Nonstationary effects in the abel transform. *IEEE Transactions on Information Theory*, 34:158–161, 1988.

[41] T.P. Wangler. Relation between field energy and rms emittance in intense particle beams. In *Proceedings of the 1985 IEEE Particle Accelerator Conference*, New York, 1985. IEEE.